

1 We would like to thank the Editor for the helpful comments that led to a significant  
 2 improvement of the manuscript. We accepted all your minor suggestions, except a couple of  
 3 comments for which we clarified the motivations in the list below. We attach a complete list of  
 4 your questions/comments with the specific reply and the marked-up version of the manuscript.  
 5

6 **RESPONSE TO THE EDITOR**

NOTES	CORRECTIONS
<i>Page 1, line 23. elevation changes brought about by</i>	We didn't analyze only the elevation changes, but also the surface displacements. Therefore, we prefer to keep the sentence as is.
<p><i>Page 1 line 24. I suggest you add some text saying something like overall patterns of elevation loss and gain are similar and the magnitude of changes are within X %.</i></p> <p><i>Also summarize here, in one sentence the extent to which the SfM was able to reproduce the patterns and magnitudes of displacement of the rock glacier observed by the ALS.</i></p>	As suggested we added the range of the elevation loss and gain on the glacier and we reported the magnitudes of the displacements for the rock glacier.
<i>Page 1 line 31. include some of your recommendations here?</i>	As suggested we added some recommendations in the text.
<i>Page 3 line 79. explain this acronym</i>	We define it.
<i>Page 3 line 88. explain briefly what you mean by "direct glaciological method" for non-glaciologists.</i>	As suggested, we clarified the concept adding a reference. We remove the term 'direct' in the entire manuscript.
<i>Page 3 line 89. explain w.e. means water equivalent here.</i>	We explained it.
<i>Page 4. line 104. summarise the main results here, overall patterns and speeds.</i>	We included the average surface displacements; the activity of the rock glacier (like the two active lobes with the advance of the front of the southern lobe) is already described before.
<i>Page 4, line 117. when you say "affine transformation" are you referring to the ICP transformation below? If so change for consistency. Otherwise please explain this additional step.</i>	Our apologies, we changed it.
<i>Page 4, line 120. I assume the papers cited above in fact found these accuracies were</i>	Thank you, we accepted your suggestion.

*indeed sufficient. If so I suggest making this statement stronger by applying my changes.*

*Page 4, line 122. cite Benatone and glacier mass balance reference.* We added the references of Bertone and Carturan, 2016 for the glacier mass balance.

*Page 5, line 141. "the elevation of the survey" is not clear, do you mean "elevation of the camera positions" or "elevations recorded by the survey"?* Thank you, we mean the elevation of camera positions. We changed accordingly.

*Page 5, line 153. "Rock Glacier" is sometimes capitalised and sometimes written "rock glacier" - please be consistent. You may use Rock Glacier when you are referring to the name "AVDM3 Rock Glacier", but on its own use "rock glacier".* Our apologies, we changed accordingly. We corrected the capital letter of the "La Mare Glacier" and "AVDM3 Rock Glacier" in the text and in the figures as well.

*Page 5, line 158. For all surveys can you say at what times of day the photos were taken to give readers an idea of the potential for shadows (as you say there were no clouds)* We reported the time of the all survey in Table 2 and we included this information in the text.

*Page 6, line 180. explain exactly how this was done, or cite a relevant publication.* We clarified this by extending the explanation.

*Page 6, line 193, 196. please explain what procedures are included in denoising and cite references if appropriate. Specify which specific tool was used. how were they down-sampled? thinning? gridded means?* Our apologies; we reported the tools used for denoising and subsampling the point cloud.

*Page 6, line 196.*

*Page 7, line 198. make the citation to Opals the first time ICP matching is mentioned (in the ALS section) and remove from here.* We moved the citation of OpalsICP at page 4, line 123.

*Page 7, line 218. what is the baseline?* We defined it.

*Page 7, line 224. delta-V does not appear in your equation below* Our apologies, we corrected accordingly.

*Page 7, line 226. if delta-z is the average elevation change, then this equation does not give the total volume change as stated above, but the average volume change. Clarify.* We clarified the sentence, however we consider correct the term 'total volume change'.

*Page 8, line 231. of the glacier ice.* We clarified the sentence but it is not correct to report the glacier ice, as suggested,

because also snow is part of the measured density.

*Page 8, line 236. explain explicitly how the delta-z values were corrected.*

We clarified the concept.

*Page 8, line 242. did you use the orthoimages as well? if so say so.*

We didn't use the orthoimages to identify the features but only the hillshaded DEMs as reported in the text.

*Page 9, line 266. not here, move to sect 4.3.1*

We moved the sentence accordingly (page 13, line 420).

*Page 9, line 284. if significance is at 0.05 I don't think this can be called a "strong" correlation.*

We agree, and we changed accordingly.

*Page 9, line 285. you mean R-squared?*

We referred to the R value in order to highlight the sign (positive or negative) of the correlation.

*Page 10, line 294. this text should be in methods*

As suggested, we moved the sentence, accordingly (page 8, line 231).

*Page 10, line 301. r-squared?*

We referred to R as explained before.

*Page 10, line 304. is this a positive or negative correlation?*

This is a positive correlation, We reported the R value to highlight the positive correlation.

*Page 10, line 307. explain the viewshed analyses in methods.*

As suggested, we moved the sentence about the viewshed analysis in section 3.3 (page 8, line 234).

*Page 10, line 311. this text should be in methods*

As suggested, we moved this part in the method (page 8, line 237).

*Page 10, line 315. there is no figure 4b?*

*Page 10, line 320. bundle adjustment is not explained in the methods... either explain in methods, or explain briefly here.*

As suggested, we clarified the concept of bundle adjustment in section 3.2.2 (page 6, line 195) reporting a reference.

*Page 11, line 328. Methods*

As suggested, we moved this part in the method (page 8, line 246).

*Page 11, line 354. you should explain somewhere why you did not do the same number of analyses for the rock glacier as for the glacier. no viewshed, depth, etc analyses.*

We agree, and we clarified this in the section 3.3 (page 8, line 249).

<i>Page 12, line 366. this text should be in the methods. as well as text describing the azimuth calculations</i>	As suggested we moved this text in the section 3.3 (page 8, line 252). We provided the link used to calculate the sun angles at the time of survey.
<i>Page 12, line 389. do you mean ALS here, or photogrammetric?</i>	Our apologies, we meant SfM-MVS, thank you.
<i>Page 13, line 417. I suggest you quote the order of magnitude ranges for the velocity here in brackets to help the reader</i>	As suggested we reported the average range of surface velocity.
<i>Page 14, line 429. You should add the caveat in this section, that if someone were to survey a glacier or rock glacier which had not previously been covered by LiDAR, then they would have to invest more time in measuring the GCPs (and possibly placing marks if they used non-natural targets).</i>	Thank you, we extended the sentence as suggested.
<i>Page 14, line 431. for comparison, perhaps you might be able to estimate the processing time for the LiDAR surveys?</i>	As suggested we reported an estimation of the processing time for the LiDAR data.
<i>Page 14, line 441. to better demonstrate that these are "almost identical" you should report the error on the mean.</i>	As suggested we reported the error on the mean and we discuss the obtain results (page 16, line 493).
<i>Page 14, line 445. instead of saying "good results", be specific - what was "good" about the results?</i>	As suggested we clarified the sentence.
<i>Page 14, line 451. be specific - what were their findings? you might need to add another sentence.</i>	We extended the sentence reporting the results of Gómez-Gutiérrez et al.
<i>Page 15, line 473. it would be useful to indicate a percent areal coverage.</i>	We included the percentage.
<i>Page 16, line 495. specify whether the dGPS should be used to derive the GCP, or the camera positions (or both).</i>	We clarified the concept.
<i>Page 17, line 523. directly compare the numbers from the ALS and the SfM here, rather than just saying "reliable"</i>	As suggested, we reported the obtain results in term of average surface change and displacements rates.
<i>Page 24, Table 1. does the dash mean "not known"? If so, then say so in the caption.</i>	Thank you. We clarified in the caption.

<i>Page 24, Table 2, Caption. spell out what ICP means.</i>	We spell out the acronym.
<i>Page 25, Table 3, Caption. say this is for La Mare glacier</i>	We clarified accordingly.
<i>Page 25, Table 3, Caption. Entire</i>	We preferred to keep the sentence as is and we clarified the concept.
<i>Page 25, Table 4. To better demonstrate that the values for SfM-MVS and ALS are close it would be great if you could also show the standard error on the mean</i>	As suggested we reported the standard error of the geodetic mass balance calculation.
<i>Page 28, Figure 3. Please make legend similar to Fig. 2, so it is readable</i>	We upload the new figure modified accordingly.
<i>Page 27, Figure 4. you say DTM in the figure, but DEM in the caption, which do you mean?</i>	We upload the new figure modified accordingly.
<i>Page 30, Figure 7. what do the shaded areas mean on the graphs? Say in the caption</i>	Thank you. We clarified in the caption.
<i>Page 31, Figure 9. x-axis should read something like "number of cameras able to view a pixel"</i>	We upload the new figure modified accordingly.
<i>Page 34, Figure 16. x-axis label should say "Hillshade value"</i>	We upload the new figure modified accordingly.

7  
8  
9  
10  
11  
12  
13  
14  
15

# 16 Suitability of ground-based SfM-MVS for monitoring glacial 17 and periglacial processes

18 L. Piermattei<sup>1</sup>, L. Carturan<sup>1</sup>, F. de Blasi<sup>1</sup>, P. Tarolli<sup>1</sup>, G. Dalla Fontana<sup>1</sup>, A. Vettore<sup>2</sup> and  
19 N. Pfeifer<sup>3</sup>.

20 <sup>1</sup>Department of Land, Environment, Agriculture and Forestry, University of Padova, Italy

21 <sup>2</sup>Interdepartment Research Center of Geomatics, University of Padova, Italy

22 <sup>3</sup>Department of Geodesy and Geoinformation, TU Wien, Austria

23 Correspondence to: L. Piermattei (livia.piermattei@studenti.unipd.it)

24

## 25 Abstract

26 Photo-based surface reconstruction is rapidly emerging as an alternative survey  
27 technique to LiDAR (light detection and ranging) in many fields of geoscience fostered  
28 by the recent development of computer vision algorithms such as Structure from  
29 Motion (SfM) and dense image matching such as Multi-View Stereo (MVS). The  
30 objectives of this work ~~was~~ are to test the suitability of the ground-based SfM-MVS  
31 approach for calculating the geodetic mass balance of a 2.1 km<sup>2</sup> glacier and for ~~the~~  
32 ~~detection~~~~ing~~~~of~~ the surface displacement ~~rate~~ of a neighbouring active rock glacier  
33 located in the Eastern Italian Alps. The photos were acquired in 2013 and 2014 using  
34 a digital consumer-grade camera, ~~organizing~~~~during~~ single-day field surveys. Airborne  
35 laser scanning (ALS, otherwise known as airborne LiDAR) data were used as  
36 benchmarks to estimate the accuracy of the photogrammetric digital elevation models  
37 (DEMs) and the reliability of the method. The SfM-MVS approach enabled the  
38 reconstruction of high-quality DEMs, which provided estimates of glacial and  
39 periglacial processes similar to those achievable ~~by using~~ ALS. In stable bedrock areas  
40 outside the glacier, the mean and the standard deviation of the elevation difference  
41 between the SfM-MVS DEM and the ALS DEM was -0.42 m ± 1.72 m and 0.03 m ±  
42 0.74 m in 2013 and 2014, respectively. The overall pattern of elevation loss and gain  
43 on the glacier were similar between both methods, ranging between - 5.53 m and +  
44 3.48 m. In the rock glacier area, the elevation difference between the SfM-MVS DEM  
45 and the ALS DEM was 0.02 m ± 0.17 m. The SfM-MVS was able to reproduce the  
46 patterns and the magnitudes of displacement of the rock glacier observed by the ALS,  
47 ranging between 0.00 m and 0.48 m per year.

48 The use of natural targets as ground control points, the occurrence of shadowed and  
49 low-contrast areas, and in particular the sub-optimal camera network geometry  
50 imposed by the morphology of the study area were the main factors affecting negatively  
51 the accuracy of photogrammetric DEMs. Technical improvements such as using aerial  
52 platform and/or placing artificial targets could significantly improve the results, but risk  
53 to be more demanding in terms of costs and logistics.

54

## 55 **1. Introduction**

56 Knowledge of changes in the extent, mass and surface velocity of glaciers and rock  
57 glaciers contributes to better understanding the dynamic processes occurring in cold  
58 high-mountain environments and serves as an important contribution to climate  
59 monitoring (Kääb et al., 2003). Numerous techniques exist for monitoring and  
60 quantifying these changes and include both field and remote sensing methods  
61 (Immerzeel et al., 2014). Fieldwork generally yields high-quality data but with a small  
62 spatial extent, given the remoteness and low accessibility of mountain areas at high  
63 elevations (Roer et al., 2007). Therefore, using remotely sensed datasets for at least  
64 two different points in time has become an important tool for monitoring high-mountain  
65 terrain dynamics (Kääb, 2002). Multitemporal Digital Elevation Models (DEMs) based  
66 on remote sensing data are the most commonly used products for such investigations  
67 (Kääb, 2005; Tseng et al., 2015).

68 Among the available remote sensing techniques, ~~the~~ close-range photogrammetry ~~saw~~  
69 has experienced a rapid development thanks to the recent ~~evolution of~~ progress in  
70 digital photogrammetry, based on computer vision algorithms. This technique is  
71 becoming the major alternative to traditional surveying techniques and LiDAR (light  
72 detection and ranging) technologies, due to its lower cost, high portability, and easy  
73 and rapid surveying in the field.

74 The photogrammetric approach known as Structure from Motion (SfM) allows ~~obtaining~~  
75 3D information of the photographed object to be obtained from a sequence of  
76 overlapping images taken with a digital camera. There are only a limited number of  
77 ~~applications-examples whereof~~ SfM photogrammetry has been applied in glacial and  
78 periglacial environments ~~exists~~, and ~~they~~ these studies principally involve the use of  
79 Unmanned Aerial Vehicles (UAVs) for image acquisition (Solbø S. and Storvold R.  
80 2013; Whitehead et al., 2013; Immerzeel et al., 2014, Tonkin et al., 2014; Gauthier et

81 al., 2014; Bühler et al., 2014; Dall’Asta et al., 2015; Ryan et al., 2015) rather than  
82 ground-based surveys (Gómez-Gutiérrez et al., 2014; 2015; Käab et al., 2014;  
83 Piermattei et al., 2015).

84 The objective of our work ~~was~~ to assess the suitability of the ground-based SfM  
85 approach for monitoring glacial and periglacial processes in a high-altitude area of the  
86 Ortles-Cevedale Group (Eastern Italian Alps). In particular, this approach was used to  
87 calculate the geodetic annual mass balance of a 2.1 km<sup>2</sup> glacier and to detect the  
88 surface displacement of a neighbouring 0.06 km<sup>2</sup> rock glacier. The photogrammetric  
89 surveys were intentionally planned to be as quick and cost-effective as possible, and  
90 easily replicable in the future. Therefore, a consumer-grade camera was ~~adopted to~~  
91 ~~find~~used in order to strike an appropriate balance between i) the affordability and  
92 accessibility of the system (i.e. cost and ease of use) and ii) the quality of the resulting  
93 topographic data (accuracy and measurement density). The accuracy of the  
94 photogrammetric DEMs was ~~estimated using~~assessed by comparison to ALS-based  
95 DEMs acquired ~~during the same periods~~within 3 weeks or less of they survey. The  
96 main factors affecting the accuracy of the photogrammetric DEMs were investigated,  
97 and the significance of the biases in the quantification of glacial and periglacial  
98 processes was discussed.

99

## 100 2. Geographical setting and case studies

101 The La Mare Glacier and the neighbouring AVDM3 (Alta Val de la Mare, 3<sup>rd</sup>; Carturan  
102 et al., 2015) Rock Glacier are located in the south-eastern part of the Ortles-Cevedale  
103 massif (Eastern Italian Alps), the largest glaciated mountain group of the Italian Alps  
104 (Fig. 1).

105 The La Mare Glacier (World Glacier Inventory code I4L00102517; WGMS 1989) is a  
106 3.55 km<sup>2</sup> valley glacier currently composed of two ice bodies, which have different  
107 morphologies and tend to separate (Carturan et al., 2014). In this work, the focus was  
108 on the southern ice body, which feeds the main tongue. This 2.1 km<sup>2</sup> ice body primarily  
109 faces north-east, and its surface is rather flat, with the exception of the small remnant  
110 of its valley tongue. The elevation ranges from 2660 to 3590 m a.s.l. Mass balance  
111 investigations using the ~~direct~~ glaciological method, based on in-situ measurements of  
112 surface ablation and accumulation (Østrem and Brugman, 1991) were started on La  
113 Mare Glacier in 2003 and detected an average annual mass balance of -0.76 m ~~w.e.~~

114 ~~y<sup>-4</sup>~~ water equivalent per year (w.e. y<sup>-1</sup>) during the period from 2003 to 2014 (Carturan,  
115 2016). The mass balance was close to zero in 2013 (-0.06 m w.e.) and was positive  
116 for the first time since the beginning of measurements in 2014 (+0.83 m w.e.).  
117 The AVDM3 Rock Glacier (Carturan et al., 2015) is an intact, tongue-shaped rock  
118 glacier characterized by the presence of two lobes. The 0.058 km<sup>2</sup> wide ~~r~~Rock ~~g~~Glacier  
119 (maximum length of 390 m; maximum width of 240 m) faces south-east and is located  
120 at elevations of between 2943 and 3085 m a.s.l. The average slope of the ~~r~~Rock  
121 ~~g~~Glacier is 26°, and the slope of the advancing front is 36°. The activity status of the  
122 AVDM3 Rock Glacier was assessed via repeated geomorphological field surveys  
123 between 2007 and 2014. These surveys revealed the advance of the front of the  
124 southern lobe (Carturan, 2010). The general morphology and the elevation of the front  
125 also suggest that this rock glacier is active (Seppi et al., 2012), and its ~~permafrost~~  
126 ~~content state~~ is further corroborated by spring temperature measurements (Carturan  
127 et al., 2015). Moreover, Bertone (2014) provided the first quantification of the surface  
128 displacement rates of this rock glacier ~~for~~ from 2003 to 2013 using ALS data, averaging  
129 8 cm yr<sup>-1</sup>.

130

### 131 **3. Methods**

#### 132 **3.1 The ALS data**

133 ALS flights of the study area were available for 17 September 2003, 22 September  
134 2013, and 24 September 2014. The technical specifications of the three ALS surveys  
135 are reported in Table 1. To avoid errors due to global shifts or rotations between the  
136 individual DEMs, the ALS point clouds were automatically co-registered using a  
137 version of the ICP algorithm (Chen and Medioni, 1991; Besl and McKay, 1992) tailored  
138 to topographic point clouds (OpalsICP, TU Wien, Glira et al., 2015). The LiDAR point  
139 cloud acquired in 2013 was treated as a reference only for stable areas outside the  
140 glaciers, rock glaciers, snow patches, and geomorphologically active areas (e.g.,  
141 landslides, river beds, and debris flows). The 2003 and 2014 LiDAR point clouds were  
142 iteratively fitted to the reference point cloud by applying an affine-ICP transformation.  
143 The ICP registration of the point clouds produced z-direction residual values of 0.08 m  
144 and 0.11 m for the 2014 and 2003 LiDAR point clouds, respectively. These accuracies  
145 ~~can be assumed~~ were found to be sufficient for calculating the annual elevation

146 changes of the glacier and the decadal displacement rate on the rock glacier ([Bertone,](#)  
147 [2014; Carturan, 2016](#)).

148 The co-registered point clouds were then converted to DEMs using Natural Neighbours  
149 interpolations. A pixel size of 1 x 1 m was produced for the La Mare Glacier, whereas  
150 a pixel size of 0.5 x 0.5 m was used for the rock glacier, based on the LiDAR point  
151 cloud density (Fig. 2). To evaluate the relative ALS DEM accuracies after the co-  
152 registration, the elevation difference errors of the DEMs were calculated for the stable  
153 areas. The standard deviation from the 2013 ALS DEM was 0.19 m and 0.21 m for the  
154 2014 and 2003 DEM comparisons, respectively.

155

## 156 **3.2 The photogrammetric workflow**

### 157 **3.2.1 Field surveys**

158 The terrestrial photogrammetric surveys of the La Mare Glacier were conducted on 4  
159 September 2013 and 27 September 2014, that is, close to the end of the mass balance  
160 year and [theef](#) ALS flights. The timing of the surveys enabled the calculation of the  
161 annual mass balance of the glacier and to compare the results with the ALS-based  
162 results. On both days, the sky was clear, with almost no cloud cover.

163 To guarantee a safe and easily repeatable survey of the glacier, the direct access to  
164 its surface was avoided and the survey was performed from a rocky ridge on the north  
165 side of the glacier (Fig. 5). The elevation of the [survey camera positions](#) ranged from  
166 3100 to 3300 m in 2013 and from 2600 to 3300 m in 2014. The distance from the  
167 glacier surface to the camera positions dictated by the topography ranged between  
168 300 and 2900 m. To cover the entire glacier surface from these positions, the acquired  
169 images were panoramic, which involved taking a series of photographs rotating the  
170 camera from each individual camera position. In 2013, seven camera positions were  
171 used, and 37 photographs were taken with the camera attached to a small tripod to  
172 avoid camera shake. In 2014, the number of camera positions was increased to 21,  
173 and 177 photos were taken freehand (Fig. 3, [Table 2](#)).

174 Both surveys were performed [in the morning, avoiding the hours with too high solar](#)  
175 [zenith angle \(Table 2\)](#), using a SLR Canon EOS 600D. The camera was equipped with  
176 a 25-70 mm zoom lens, which was set to a focal length of 25 mm in 2013 and 35 mm  
177 in 2014.

178 The terrestrial photogrammetric survey of the AVDM3 Rock Glacier was performed on  
179 27 September 2014, between 12:15 and 14:00 (local solar time). In this survey, 198  
180 images were acquired freehand while walking around and on top of the rock glacier.  
181 The survey camera was a CANON EOS 5D full frame SLR camera equipped with a  
182 fixed-focal lens of 28 mm. The photographs were acquired and saved in RAW format  
183 in both surveys.

184

### 185 **3.2.2 Data processing**

186 The photogrammetric approach, based on SfM algorithms, can automatically derive  
187 the 3D position of an object in images taken in sequence calculating the camera  
188 parameters (intrinsic and extrinsic) (Hartley and Zissermann, 2004). Dense image  
189 matching algorithms are then used to reconstruct the 3D model of the object as a dense  
190 point cloud. Multiple photogrammetric packages implementing SfM and Multi-View  
191 Stereo (MVS) algorithms for dense image matching exist, and in this work, the software  
192 PhotoScan Pro (AgiSoft LLC. 2010a) was used. Henceforth, the photogrammetric  
193 surveys and results are referred to using the acronym SfM-MVS.

194 The photo-based reconstruction workflow is summarized in Fig. 4. The key  
195 components of the workflow are 1) acquisition and photograph editing, 2) GCPs  
196 identification, image feature detection, matching and 3D scene reproduction (the SfM-  
197 MVS steps), 3) point cloud processing, (filtering, subsampling and ICP) and 4) DEM  
198 reconstruction.

199 To overcome the significant variability in brightness during the surveys, the RAW  
200 images have been edited to adjust the exposure and contrast in order to retrieve  
201 information from the overexposed (e.g., snow-covered) areas and underexposed (e.g.,  
202 shadowed) areas. These editing steps had a positive impact on the number of image  
203 features extracted. The edited images were saved in TIFF format and loaded in  
204 PhotoScan where non-stationary objects (i.e., clouds and shadows), the sky, and  
205 features lying in the distant background have been masked.

206 The camera calibration parameters were calculated ~~using artificial targets~~ prior to the  
207 processing of the photogrammetric surveys ~~(pre-calibrated camera)~~. The camera was  
208 calibrated in a field test area, using artificial targets surveyed by Total Station and  
209 maintaining the same camera setting adopted during the photogrammetric surveys.

210 The calculated intrinsic parameters were kept constant during the bundle adjustment

211 ~~optimization (Triggs et al., 1999) entire SfM processing~~ given the limits of the camera  
212 network geometry and the homogeneous texture of the surveyed terrain. As additional  
213 constraint, ~~the~~ GCPs were included into the SfM process to avoid instability in the  
214 bundle adjustment solution (Verhoeven et al., 2015). The GCPs were selected to be as  
215 natural features in stable areas outside the glacier and rock glacier, and their  
216 coordinates were extracted from the 2013 ALS hillshaded DEM. After the SfM step,  
217 the geo-referenced dense point cloud was reconstructed by the MVS algorithm, using  
218 the 'mild' smoothing filter to preserve as much spatial information as possible (AgiSoft  
219 LLC., 2010b).

220 To reduce the noise and outliers generated during the dense matching reconstruction  
221 (Bradley et al., 2008; Nilosek et al., 2012), an initial filtering was performed in  
222 PhotoScan to manually remove the outliers. Further denoising was applied to the  
223 dense point clouds exported from PhotoScan, using ~~a a specific tool to treat tool~~  
224 implemented in the open source software CloudCompare, based on the statistical  
225 approach called S.O.R. (Statistical Outlier Removal). To obtain a uniform spatial  
226 distribution of the points, the photogrammetric point clouds (much denser than the ALS  
227 point clouds), were down-sampled to 20 cm for the glacier and 10 cm for the rock  
228 glacier, using the Spatial subsampling tool of CloudCompare. Following the same  
229 procedure used for the ALS data, the ICP algorithm (~~OpalsICP, TU Wien~~) was applied  
230 to co-register the point clouds in the stable area outside the glacier and rock glacier,  
231 using the 2013 ALS point cloud as a reference. The co-registered point clouds were  
232 then converted to DEMs, using ~~the~~ Natural Neighbours interpolation and the same  
233 pixel sizes as of the ALS DEMs (i.e., 1 x 1 m for the glacier and 0.5 x 0.5 m for the rock  
234 glacier). The data acquisition settings and processing results of the photogrammetric  
235 surveys are summarized in Table 2.

236

### 237 **3.3 Analyses**

238 The accuracy of the photogrammetric DEMs was assessed by calculating the mean,  
239 the mean of the absolute values and the standard deviation ( $\sigma$ ) of the elevation  
240 differences (DEM of Difference, DoD) between SfM-MVS DEMs and ALS DEMs, using  
241 the latter as a reference dataset. For both surveyed areas, the primary factors  
242 controlling the quality of the photogrammetric results (~~i.e., camera-object distance,~~  
243 ~~slope and angle of incidence, camera network geometry, surface texture and shadows~~)  
244 were evaluated in terms of DEM accuracy and spatial resolution. For the La Mare

245 Glacier area, the role of slope, angle of incidence, camera-object distance, camera  
246 network geometry and surface texture was analysed. The role of the incidence angle  
247 between the line of sight of the camera and the photographed object (vector normal to  
248 the surface), was investigated by analysing the mean angles calculated from five  
249 representative camera locations at different elevations. Because the redundancy of the  
250 observations, that is the number of cameras that view the same point on the glacier,  
251 influences the quality of the photogrammetric results, a viewshed analysis was carried  
252 out calculating the number of cameras able to see each pixel. The effect of the camera-  
253 object distance (i.e., depth, Gómez-Gutiérrez et al., 2014), was evaluated by  
254 calculating the accuracy for pixels clustered in 200 m distance classes from a camera  
255 position at the centre of the array displayed in Figure 5b. The obtained results were  
256 compared to the theoretical behaviour of the error as a function of the depth ( $\sigma_d$ ),  
257 calculated using the following formulation:

$$258 \quad \sigma_d = m_B \cdot \frac{D}{B} \cdot \sigma_i, \quad (1)$$

259 where  $m_B$  represents the image scale ( $D / \text{focal length}$ );  $D$  is the depth (camera-object  
260 distance);  $B$  is the baseline (i.e., the distance between each pair of adjacent camera  
261 positions) and  $\sigma_i$  is the measured accuracy in the image space. The accuracy of  
262 photogrammetric reconstructions for the different substrata was then evaluated,  
263 outlining each substratum on the orthophoto exported from PhotoScan.

264 For the rock glacier area, only the effect of slope and shadow areas on the accuracy  
265 of the SfM DEM was evaluated, as others factors like the camera-object distance and  
266 the incidence angle cannot be reliably quantified due to the different ground survey  
267 characteristics (i.e. the photos were acquired by walking on the target). As suggested  
268 by Gómez-Gutiérrez et al., (2014), the relationship between the quality of the  
269 photogrammetric DEM and the amount of shadowed-lighted areas in the photographs  
270 was calculated using a hillshaded model that was calculated by simulating the azimuth  
271 and zenith angles position of the sun in the sky during the survey (azimuth and zenith  
272 angles) (Astronomical Applications tool).

273 After the accuracy assessments, we investigated the suitability of using the terrestrial  
274 photogrammetric surveys to calculate the annual mass balance of the glacier and the  
275 surface displacement rates of the rock glacier, comparing the results with those  
276 obtained from ALS surveys. The mass balance and elevation changes were calculated  
277 by differencing multitemporal DEMs.

278 The geodetic mass balance was calculated from the total volume change  $\Delta V$  (m<sup>3</sup>) of  
279 the glacier between two survey dates:

$$280 \quad \Delta V = \overline{\Delta z} \cdot A \quad (2)$$

281 where  $\overline{\Delta z}$  is the average elevation change between two DEMs over the area  $A$  of the  
282 glacier. The area-averaged net geodetic mass balance in metres of water equivalent  
283 per year (m w.e. y<sup>-1</sup>) was calculated as:

$$284 \quad \dot{M} = \frac{\Delta V \cdot \rho}{A} \quad (3)$$

285 where  $\rho$  is the mean density. ~~The area  $A$  of the glacier between the two surveys did~~  
286 ~~not change. The mean density was~~ obtained by a fractional area-weighted mean,  
287 assigning 900 kg/m<sup>3</sup> for the ablation area (Huss, 2013) and 530 kg/m<sup>3</sup> for the  
288 accumulation area, as directly measured in a snowpit. The resulting weighted mean  
289 density was 600 kg/m<sup>3</sup>. The area  $A$  of the glacier between the two surveys did not  
290 change. In the mass balance calculations we used both raw  $\overline{\Delta z}$  values and ~~corrected~~  
291  $\overline{\Delta z}$  values ~~corrected by removing the used to account for the~~ mean errors in the stable  
292 areas outside the glacier ~~(, as reported in Table 3).~~ Other processes like ice fluxes,  
293 varying snow density and re-freezing of melt water were assumed to be negligible for  
294 the calculation of the annual geodetic mass balance (Zemp et al., 2013).

295 The horizontal surface displacements rates of the AVDM3 ~~R~~rock ~~G~~glacier were  
296 estimated by a manual measurement of the displacement of single boulders identified  
297 in the hillshaded DEMs. Several points were also located outside the rock glacier to  
298 assess the accuracy of the surface velocity determinations. Displacements in the  
299 horizontal plane were analysed instead of 3D displacements, which are affected by  
300 surface elevation changes (Isaksen et al., 2000).

301

## 302 **4. Results**

### 303 **4.1 Accuracy assessment on the area of La Mare Glacier**

304 The mean elevation difference between the SfM-MVS DEM from 4 September 2013  
305 (Fig. 5a) and the ALS DEM from 22 September 2013 (Fig. 2b), evaluated in the  
306 common stable area outside the glacier, was -0.42 m ( $\sigma = 1.72$  m). The same  
307 calculation between the SfM-MVS DEM from 27 September 2014 (Fig. 5b) and the

308 ALS DEM from 24 September 2014 (Fig. 2a) yielded a mean value of 0.03 m ( $\sigma = 0.74$   
309 m). In this area, the mean difference between the 2014 and 2013 SfM-MVS DEMs is  
310 0.38 m ( $\sigma = 1.73$  m), and the mean difference between the respective ALS DEMs is -  
311 0.09 m ( $\sigma = 0.29$  m, Table 3).

312 These results show that the photogrammetric survey conducted in 2014, using a higher  
313 number of camera positions and photographs and a slightly longer focal length,  
314 provided a significant improvement compared to the survey of 2013. In addition to the  
315 higher  $\sigma$ , the 2013 SfM-MVS DEM has a residual average bias of -0.42 m, which must  
316 be taken into account in the glacier mass balance calculations. Table 3 presents the  
317 same statistics for the ~~area of data covering~~ the glacier. However, given that in 2013  
318 the ablation was not negligible between the photogrammetric survey of 4 September  
319 and the ALS survey of 22 September, the comparison between SfM-MVS and ALS of  
320 the same year is meaningful only in 2014, with a mean difference of 0.23 m ( $\sigma = 0.65$   
321 m). ~~The comparison of the two ALS DEMs of 2014 and 2013 yields a mean difference~~  
322 ~~of 1.30 m for the glacier, attributable to the positive mass balance experienced by the~~  
323 ~~glacier in that time period (+0.83 m w.e., Carturan, 2016).~~

324 The spatial distribution of the elevation difference between the SfM-MVS and ALS  
325 DEMs surveyed at the same times (Fig. 6 and 7) suggests that the most problematic  
326 areas for photogrammetric reconstructions are those that are far from the camera  
327 positions, steep, and covered by fresh snow. Certain outliers can be observed in steep  
328 areas outside the glaciers, even after filtering, but they likely have no influence on the  
329 glacier, where the slope is much lower.

330 The factors controlling the quality of the photogrammetric DEMs were investigated in  
331 detail using the SfM-MVS DEM from 27 September 2014, which has a higher spatial  
332 coverage than that of 2013 and is almost contemporaneous with the ALS DEM from  
333 24 September 2014 (which means negligible ablation and accumulation on the glacier).  
334 As expected, the standard deviation of elevation differences between the 2014 SfM-  
335 MVS and ALS DEMs is proportional to slope but remains lower than 1 m up to 40° on  
336 the glacier and up to 60° in the area outside it (Fig. 8). Grouping the data for slope  
337 classes of 10 degrees and excluding classes with less than 1000 grid cells, ~~it was~~  
338 ~~possible to calculate~~ a strong positive correlation was found between the absolute  
339 value of the elevation difference and the slope ( $R = 0.86$  both inside and outside the  
340 glacier, significant at the 0.05 level). A rapid increase in the error is observed for the  
341 highest slope classes, which represent a very small part proportion of the investigated

342 area. For the glacier, only 1% of the area has a slope higher than 40°. The mean  
343 elevation difference is around zero for most of the low- and middle-slope classes, with  
344 the exception of the 0-10° class inside the glacier, where a mean value of 0.41 m ( $\sigma =$   
345 0.44 m) was calculated. Interestingly, the majority of this slope class lies in a flat area  
346 of the glacier at 3200-3300 m a.s.l. and is covered by fresh snow, which has poor  
347 texture. In addition, this zone has an unfavourable line of sight from the camera  
348 positions.

349 ~~The role of the incidence angle between the line of sight of the camera and the~~  
350 ~~photographed object (vector normal to the surface), was investigated by analysing the~~  
351 ~~mean angles calculated from five representative camera locations at different~~  
352 ~~elevations.~~ In the glacier area, ~~where~~ most of the mean incidence angles ranges  
353 between 70° and 90° (75%, Figure 9a). The scatterplot of elevation differences  
354 between the 2014 SfM-MVS and ALS DEMs versus the mean incidence angles  
355 calculated for every pixel shows no statistically significant relationship ( $R = 0.21$ ).  
356 However, by analysing this relationship for classes of incidence angle, and considering  
357 the mean of the elevation differences in absolute value and the classes with more than  
358 1000 pixels, yields a correlation coefficient  $R = 0.95$  (significant at the 0.05 level).

359 ~~Because the redundancy of the observations, that is the number of cameras that views~~  
360 ~~the same points on the glacier, influences the quality of the photogrammetric results,~~  
361 ~~a viewshed analysis was carried out (Fig. 9d).~~ The results of the viewshed analysis  
362 (Fig. 9d) show anti-correlation between the absolute value of elevation difference and  
363 the number of cameras viewing reconstructed pixels (Fig. 9e), yielding a coefficient of  
364 correlation of -0.63, which is significant at the 0.05 level.

365 ~~The effect of the camera-object distance (i.e., depth, Gómez-Gutiérrez et al., 2014),~~  
366 ~~was evaluated by calculating the mean and standard deviation of the elevation~~  
367 ~~difference between the 2014 SfM-MVS and ALS DEMs, clustering the pixels in 200 m~~  
368 ~~distance classes from a camera position at the centre of the array displayed in Figure~~  
369 ~~4b.~~ The relationship between error and depth is clearer for the glacier area (Fig. 10a),  
370 whereas in the surrounding bare ground area, the error appears to be more influenced  
371 by the variability of the slope angle (Fig. 10b).

372 The theoretical  $\sigma_d$  was calculated using Eq. 1 for each class of distance, considering a  
373 mean baseline of 400 m and an accuracy in the image space of 0.40 pixel, which is  
374 the reprojection error after bundle adjustment ~~computations~~. Another quantification of  
375 the error as a function of the depth was obtained, for comparison purposes, by

376 multiplying the Ground Sample Distance (GSD) (which increases with depth) by the  
377 reprojection error provided by PhotoScan for the Ground Control Points. Figure 10c  
378 shows that, on the glacier, the accuracy calculated from the DoD matches quite well  
379 the 'theoretical' calculations up to a depth of 1900 m. Beyond this distance, the  
380 detected error increases faster than in theory, likely due to the increasing coverage of  
381 fresh snow, which affects the image texture and decreases the accuracy.

382 ~~The accuracy of photogrammetric reconstructions for the different substrata was then~~  
383 ~~evaluated. The spatial distribution of each substratum was outlined on the orthophoto~~  
384 ~~exported from PhotoScan.~~ Debris-, ice- and firn-covered areas display similar  
385 accuracy, with median values of elevation difference between the 2014 SfM-MVS and  
386 ALS-based DEMs close to zero and interquartile ranges of the same magnitude.  
387 Conversely, the area covered by fresh snow, which is also the area with greater depth,  
388 shows prevailing overall positive differences, a median value of 0.48 m and a much  
389 higher standard deviation ( $\sigma = 0.82$  m).

390 The texture of the surface also influences the point density distribution and the spatial  
391 coverage of the reconstructed area. A lower value of the point density was obtained  
392 for fresh snow (4 pts m<sup>-2</sup>). Increasing point densities were obtained for firn, ice and  
393 debris (10, 13 and 15 pts m<sup>-2</sup>, respectively). The spatial coverage in the fresh snow  
394 area was 75%, whereas it was 93% in the rest of the glacier. Excluding the areas not  
395 visible from the camera position and occlusions imposed by the topography, the spatial  
396 coverage in the fresh snow area was 82% and 98% in the remaining part.

397 The point density is also affected by the depth, elevation and slope (Fig. 12). Due to  
398 the GSD, the average point density decreases with depth, which in our case is also  
399 proportional to the elevation. On the glacier, the point density decreases more rapidly  
400 than in the surrounding area for elevations between 3100 and 3300 m a.s.l., due to the  
401 poor texture in this snow-covered flat area. Increasing densities with slope, up to 70-  
402 80°, are observed and likely result from more favourable incidence angles, which do  
403 not however guarantee high accuracy, as noted earlier (Fig. 9). Considering the entire  
404 reconstructed surface, the point density was higher in the area surrounding the glacier  
405 than on it (12 pts m<sup>-2</sup> vs. 8 pts m<sup>-2</sup>, respectively).

406

## 407 4.2 Accuracy assessment in the area of the AVDM3 Rock Glacier

408 The 2014 terrestrial photogrammetric survey of the AVDM3 Rock Glacier provided a  
409 good spatial coverage (83%) of high-resolution terrain data (Fig. 13). The spatial  
410 distribution of the elevation difference between the contemporaneous SfM-MVS and  
411 ALS DEMs shows the existence of areas with both positive and negative values (Fig.  
412 14). The average elevation difference is 0.02 m on the rock glacier ( $\sigma = 0.17$ ) and 0.05  
413 in the surrounding areas ( $\sigma = 0.31$  m, Tab. 5).

414 Similar to the La Mare Glacier area, the accuracy decreases with increasing slope in  
415 the rock glacier area. The standard deviation of the average elevation difference  
416 between the SfM-MVS and ALS DEMs is less than 0.20 m up to 40°. In the area  
417 surrounding the rock glacier, the error increases faster with slope because steep areas  
418 coincide with shaded areas and (because the images were acquired in the afternoon)  
419 high solar zenith angles. ~~As suggested by Gómez-Gutiérrez et al., (2014), the~~  
420 ~~relationship between the quality of the photogrammetric DEM and the amount of~~  
421 ~~shadowed-lighted areas in the photographs was calculated using a hillshaded model~~  
422 ~~that was calculated by simulating the position of the sun in the sky (azimuth and zenith~~  
423 ~~angles) during the survey. As shown in Figure 16, larger errors, indeed, occur in~~  
424 ~~shadowed rather than in areas and smaller errors in well-lit areas, even if the largest~~  
425 ~~differences in accuracy can be observed outside rather than on the rock glacier (~~  
426 ~~Fig.~~  
427 16).

427

## 428 **4.3 Glacial and periglacial processes**

### 429 **4.3.1 Mass balance of La Mare Glacier**

430 Due to abundant solid precipitation during the accumulation season and low ablation  
431 rates during the summer (the glacier was snow-covered above ~3000-3100 m a.s.l.),  
432 the mass balance of the La Mare Glacier was positive in the 2013-14 hydrological year  
433 for the first time since the beginning of measurements in 2003. ~~According to the direct~~  
434 ~~glaciological method, the annual mass balance was +0.83 m w.e. (Carturan, 2016).~~  
435 The comparison of the two ALS DEMs of 2014 and 2013 yields a mean difference of  
436 1.30 m for the glacier area, attributable to the positive annual mass balance measured  
437 by using the glaciological method experienced by the glacier in that time period (+0.83  
438 m w.e., Carturan, 2016).

439 As shown in Table 4, the geodetic mass balance estimates using only ALS data do not  
440 differ significantly for either the entire glacier or the sub-areas covered by the  
441 photogrammetric surveys of 2013 and 2014 (88% and 93%, respectively). The  
442 estimates range between 0.85 and 0.88 m w.e for the raw data and between 0.90 and  
443 0.94 m w.e. for the corrected data. The geodetic mass balance calculations using only  
444 photogrammetric data yield a raw value of 1.09 m w.e. and a corrected value of 0.87  
445 m w.e. Using the 2014 SfM-MVS, which has a higher quality than the 2013 SfM-MVS  
446 ALS-DEM, yields a raw value of 0.98 m w.e. and a corrected value of 1.02 m w.e. Area-  
447 averaged estimates of the geodetic mass balance from photogrammetric data are very  
448 close to the estimates from ALS data and from the glaciological-direct method and are  
449 closer still if the mean DEM error in the stable areas outside the glacier is subtracted  
450 from the raw average elevation differences. The spatial distribution and magnitude of  
451 elevation change is also well captured by the terrestrial photogrammetry (Fig. 17 and  
452 18), even if, as already noted in the previous section, problematic areas are present in  
453 the upper part of the glacier, which was covered by fresh snow, especially in the 2013  
454 SfM-MVS survey.

455

#### 456 **4.3.2 Surface changes and velocities of the AVDM3 Rock Glacier**

457 The spatial distribution and the mean value of elevation change on the surface of the  
458 AVDM3 Rock Glacier were calculated differencing the available SfM-MVS and ALS  
459 DEMs. Table 5 shows that, according to the ALS data, there was a prevailing an overall  
460 lowering of the surface in the period from 2003 to 2014. Taking into account the  
461 average residual bias in the stable area outside the rock glacier, the average lowering  
462 rates of the rock glacier surface were 1.5 cm y<sup>-1</sup> in the period from 2003 to 2013, and  
463 2 cm in the year 2013-14. Comparing the SfM-MVS DEM of 2014 with the ALS DEMs  
464 of 2013 and 2003 and accounting for the mean bias outside the rock glacier, we  
465 obtained slightly higher lowering rates of 2.2 cm y<sup>-1</sup> from 2003 to 2013 and 5 cm from  
466 2013 to 2014. As expected on the basis of the accuracy assessment (Section 4.2), the  
467 decadal lowering rates calculated from the SfM-MVS DEM are in closer agreement  
468 with those calculated from ALS data than the single-year calculations. The same can  
469 be observed for the spatial distribution of the elevation changes (Fig. 19), which shows  
470 an-prevailing overall thinning in the upper and middle part of the rock glacier and a  
471 thickening of the two advancing lobes. Figure 20 shows that the fastest moving areas

472 in the period from 2003 to 2014 were the two frontal lobes, which also featured the  
473 greatest elevation changes. Table 6 shows that the SfM-MVS and ALS data produced  
474 very similar surface velocities (ranging between 0.09 and 0.27 m yr<sup>-1</sup> on average) for  
475 the three sub-areas, ~~(each with homogeneous displacement,)~~ into which the rock  
476 glacier can be divided. Outside the rock glacier, the photogrammetric method exhibited  
477 a slightly lower accuracy compared to the ALS, but no systematic shift of the different  
478 DEMs was found.

479

## 480 5. Discussion

### 481 5.1 Data processing and accuracy assessments

482 The results of our terrestrial photogrammetry applications on the La Mare Glacier and  
483 on the AVDM3 Rock Glacier demonstrate that it is possible to reliably quantify the  
484 investigated glacial and periglacial processes by means of a quick and safe survey that  
485 was conducted on a single day using cheap, light and easy-to-use hardware.  
486 Moreover, time-consuming and unsafe direct access to the glacier surface was not  
487 required. However, it should be noted that, without LiDAR data coverage, more time  
488 should have been invested for surveying GCPs and possibly placing artificial markers.

489 The data processing ~~times were significantly long~~ did take a long time, however. For a  
490 single operator, the processing time is approximately 10 days, which is around twice  
491 of the time necessary for LiDAR data processing. The most labour-intensive and time-  
492 consuming tasks were the pre-processing steps i.e., masking of the photos,  
493 identification of reference points from the LiDAR DEM and then in the images, and  
494 processing of the images (the MVS step is particularly computationally intensive),  
495 which is directly related to the resolution and the number of photographs uploaded and  
496 the computer performance. Several steps required a certain degree of subjectivity,  
497 e.g., the identification of the GCPs. However, due to the high automatism of the image  
498 processing, the level of expertise is considerably lower than for LiDAR and traditional  
499 photogrammetry.

500 On the La Mare Glacier, the area-averaged estimates of the 2013-14 geodetic mass  
501 balance from ALS and photogrammetric data were almost identical ( $0.91 \pm 0.16$  and  
502  $0.87 \pm 1.30$  m w.e., respectively) and close to the mass balance calculated from the  
503 ~~direct~~ glaciological method ( $0.83 \pm 0.26$  m w.e.). The differences are well within the

504 uncertainty of the ~~direct glaciological and geodetic~~ mass balance estimates, which  
505 ~~was were~~ quantified following Zemp et al. (2013). in 0.26 m w.e. y<sup>-1</sup> by Carturan (2016).  
506 These results confirm that the reliable mass balance estimates ~~good results~~ obtained  
507 by Piermattei et al., (2015) on the small Montasio Glacier, in the Julian Alps, can also  
508 be replicated on larger glaciers with different morphologies and characteristics. The  
509 error of the geodetic estimates has been calculated in bare ground areas outside the  
510 glacier, where the slope is lower than the 95° percentile of the slope frequency  
511 distribution inside the glacier (i.e. 40°), and under the conservative hypothesis that the  
512 standard error of the elevation differences among the DEMs is totally correlated in  
513 space. This hypothesis was adopted because there was not a sufficiently large bare  
514 ground area, with available DoD data, for analysing the scale of the spatial  
515 autocorrelation of elevation differences (e.g. Rolstad et al., 2009). As can be seen in  
516 Table 3, the significant uncertainty of the photogrammetric method can be mostly  
517 attributed to the 2013 survey, whereas the improvements of the 2014 survey led to a  
518 substantial reduction of the error.

519 Because the AVDM3 Rock Glacier exhibits ~~sed~~ quite slow annual deformation and  
520 creep, we were able to calculate reliable displacement rates and area-averaged  
521 surface elevation changes ~~only~~ on a multi-year (in our case, decadal) time scale. This  
522 result confirms the findings of Gómez-Gutiérrez et al. (2014), who applied a similar  
523 method to the Corral del Veleta Rock Glacier in the Sierra Nevada (Spain) observing  
524 that these technique is suitable for medium-term (from 5 to 10 years intervals)  
525 monitoring of rock glacier surface displacements.

526 Our results are promising, despite the limitations of the adopted method, which include  
527 i) the location of GCPs on natural targets outside the investigated glacier/rock glacier,  
528 ii) the presence of areas with deep shadows and changes in the light during the survey,  
529 iii) the presence of fresh snow in the upper and middle part of the glacier, and iv) the  
530 high camera-object distance in the glacier application.

531 In general terms, the photo-based accuracy is related to the image feature extraction,  
532 feature matching (in both the SfM and MVS steps), and scale definition (Bemis et al.,  
533 2014). A low accuracy in these steps, caused for example by poor camera network  
534 geometry, can generate model distortion and reduce the ability to identify unique  
535 corresponding features in overlapping images (Wackrow and Chandler, 2011;  
536 Dall'Asta et al., 2015, Favalli et al., 2012; James and Robson, 2012; 2014;  
537 Hosseinaveh et al, 2014; Micheletti et al., 2014; Nocerino et al., 2014). In our case

538 studies, among the various aspects analysed, the spatial variability of the accuracy of  
539 the photogrammetric DEMs is related to the camera-object distance, the presence of  
540 fresh snow with low contrast, the changing illumination during the survey and the  
541 occurrence of shadows. The increasing error with increasing terrain slope suggests  
542 the persistence of a small shift in the reconstructed DEMs. This shift, however does  
543 not affect the areal estimates of mass balance and elevation change, given that the  
544 vast majority of the glacier and rock glacier areas feature small or moderate slope  
545 angles. For both the glacier and the rock glacier, the spatial coverage of the  
546 reconstructed areas was not complete, ranging between 72% and 85%. In the glacier  
547 surveys, the problematic areas were those visible from a low number of camera  
548 positions and those covered by fresh snow and far from the viewpoints. In the rock  
549 glacier, certain areas were not reconstructed due to the rock glacier's complex  
550 morphology and in particular to the presence of ridges, furrows and counterslopes.

551

## 552 5.2 Possible improvements of the SfM-MVS approach

553 The accuracy assessments confirm that the ALS data still provide results with  
554 somewhat higher accuracies (Tabs. 3 and 5, Figs. 6 and 14) but with much higher  
555 costs and demanding logistics than the SfM-MVS approach. However, the SfM-MVS  
556 method has the potential to provide a significantly higher spatial resolution (Debella-  
557 Gilo and Kaab, 2011; Piermattei et al., 2015) and temporal resolution due to its  
558 significantly lower costs. Moreover, the photogrammetric reconstructions still have  
559 room for improvement, as demonstrated by the better results achieved from the 2014  
560 survey of the glacier area compared to those from 2013. This improvement resulted  
561 from a higher number of photographs and improved camera network geometry.

562 Many of the limitations described above can be overcome by introducing modifications  
563 to the terrestrial photogrammetric survey strategy. For the rock glacier survey, shorter  
564 baselines are recommended to ensure greater spatial coverage, high image similarity  
565 and good matching performance (Wenzel et al., 2013). GCPs, for example, could be  
566 placed on the surface of the glaciers and rock glaciers to reduce the model distortions  
567 (Bemis et al., 2014) and generate surveys with much higher accuracies via, for  
568 example, the use of dGPS to calculate their position (Dall'Asta et al., 2015).

569 The use of UAVs could solve the problem of excessive camera-object distances and  
570 the issue of missing areas due to inaccessibility. However, these alternatives imply  
571 increased costs, more troublesome logistics, greater expertise, and ultimately longer

572 survey times. In addition, they also require directly accessing unsafe or difficult to reach  
573 areas, both to place targets and to move UAVs among study areas that exceed their  
574 operational range (Bühler et al., 2014). Therefore, the best balance must be found  
575 between simplicity, safety, costs and accuracy for each photogrammetric application  
576 based on the final objectives and on the available human and economic resources.

577

## 578 **6. Conclusions**

579 In this paper, we investigated the applicability of the SfM-MVS approach for monitoring  
580 glacial and periglacial processes in a catchment of the Ortles-Cevedale Group  
581 (Eastern Italian Alps), validating our results using ALS DEMs as benchmarks. The  
582 ground surveys were conducted on foot and were intentionally planned to be as quick  
583 and easy as possible. The 2.1 km<sup>2</sup> La Mare Glacier and the neighbouring AVDM3 Rock  
584 Glacier were surveyed in one day using only a consumer-grade SLR camera without  
585 the setup of artificial targets.

586 The accuracy of the photogrammetric DEMs, evaluated as the mean and standard  
587 deviation of the elevation difference in a stable area between the SfM-MVS DEM and  
588 the reference ALS DEM, was  $-0.42 \text{ m} \pm 1.72 \text{ m}$  and  $0.03 \text{ m} \pm 0.74 \text{ m}$  for the 2013 and  
589 2014 surveys, respectively. The SfM-MVS DEM accuracy of the reconstructed rock  
590 glacier surface acquired in 2014 was estimated to be  $0.02 \text{ m} \pm 0.17 \text{ m}$ .

591 The SfM-MVS geodetic mass balance estimates for the La Mare Glacier were in good  
592 agreement with the calculations from the contemporary ALS data and with the results  
593 of the direct glaciological method, confirming a positive mass balance of approximately  
594 0.9 m w.e. in the 2013-14 hydrological year. In the rock glacier, the survey produced a  
595 good spatial coverage of the photogrammetric DEM and a reliable calculation of the  
596 multi-year surface changes (-0.18 m on average) and displacement rates (0.18 m y<sup>-1</sup>  
597 on average) in the period from 2003 to 2014. For rock glacier applications, particularly  
598 for slow-moving ones such as AVDM3, single-year assessments of elevation change  
599 and surface velocities require the setup of artificial targets and GCPs to obtain the  
600 accuracy required to detect such slow processes.

601 The simplicity of the ground surveys and the physical characteristics of the analysed  
602 alpine terrain were the main factors influencing the tested approach. In particular, we  
603 refer to the use of natural targets as GCPs, the occurrence of shadowed areas and  
604 lighting changes during the surveys, the presence of fresh snow in the upper part of

605 the glacier (which reduced the contrast), and the sub-optimal camera network  
606 geometry and long camera-object distances imposed by the morphology and  
607 accessibility of the study area. In consideration of the factors that spatially control the  
608 accuracy of the SfM-MVS DEMs, there remains room for significant improvements,  
609 e.g., using aerial platform and/or placing artificial targets surveyed by dGPS. Further  
610 research is therefore needed to i) find technical solutions to overcome the major  
611 limitations of the SfM-MVS approach in such remote areas and ii) achieve the optimal  
612 balance between the simplicity and low cost of this approach and the accuracy required  
613 for each specific application.

614

## 615 **Acknowledgments**

616 This study was funded by the Italian MIUR Project (PRIN 2010-11): 'Response of  
617 morphoclimatic system dynamics to global changes and related geomorphological  
618 hazards' (local and national coordinators G. Dalla Fontana and C. Baroni). The authors  
619 would like to thank Philipp Glira from the TU of Wien for his precious contribution to  
620 the LiDAR data processing. The comments and suggestions from Susan Conway,  
621 Álvaro Gómez-Gutiérrez and an anonymous Reviewer have been useful for the  
622 improvement of the manuscript.

623

624

## 625 **References**

626 AgiSoft LL C: AgiSoft PhotoScan Professional Edition. Version 1.1.2, available at:  
627 <http://www.agisoft.ru/products/photoscan/> (last access: 18 January 2015), 2010a.

628 AgiSoft LL C: AgiSoft PhotoScan User-manuals Version 1.0, available at:  
629 [http://www.agisoft.com/pdf/photoscan-pro\\_1\\_1\\_en.pdf](http://www.agisoft.com/pdf/photoscan-pro_1_1_en.pdf) (last access: 15 May 2015),  
630 2010b.

631 [Astronomical Applications - U.S. Naval Observatory, Sun or Moon Altitude/Azimuth](http://aa.usno.navy.mil/data/docs/AltAz.php)  
632 [Table. Available online: <http://aa.usno.navy.mil/data/docs/AltAz.php> \(accessed on 1](http://aa.usno.navy.mil/data/docs/AltAz.php)  
633 [April 2015\).](http://aa.usno.navy.mil/data/docs/AltAz.php)

634 Bemis, S., Micklethwaite, S., and Turner, D.: Ground-based and UAV-Based  
635 photogrammetry: a multi-scale, high-resolution mapping tool for Structural Geology  
636 and Paleoseismology. *J Struct Geol.*, 69, 163–178, doi:10.1016/j.jsg.2014.10.007,  
637 2014.

638 Bertone, A.: Misure di spostamento dei rock glacier con l'uso di feature tracking  
639 applicato a DTM multitemporali, BSc Thesis, Department of Earth and Environmental  
640 Sciences, University of Pavia, Pavia, Italy, 63 pp., 2014.

641 Besl, P. J. and McKay, N. D.: Method for registration of 3-D shapes, in: Proceedings  
642 of the International Society for Optics and Photonics IEEE Transactions on Pattern  
643 Analysis and Machine Intelligence, 1611, 586–606, 1992.

644 Bradley, D., Boubekour, T., and Heidrich, W.: Accurate multi-view reconstruction using  
645 robust binocular stereo and surface meshing, in: IEEE Conference on Computer Vision  
646 and Pattern Recognition, Anchorage, AK, USA, 1–8, 2008.

647 Bühler, Y., Marty, M., Egli, L., Veitinger, J., Jonas, T., Thee, P., and Ginzler, C.:  
648 Spatially continuous mapping of snow depth in high alpine catchments using digital  
649 photogrammetry, *The Cryosphere Discuss.*, 8, 3297–3333, doi:10.5194/tcd-8-3297-  
650 2014, 2014.

651 Carturan, L.: Climate change effects on the cryosphere and hydrology of a high-altitude  
652 watershed, PhD thesis, Department of Land, Environment, Agriculture and Forestry,  
653 University of Padova, Padova, Italy, 2010.

654 Carturan, L.: Replacing monitored glaciers undergoing extinction: a new measurement  
655 series on La Mare Glacier (Ortles-Cevedale, Italy), *J. Glaciol.*, in review, 2016.

656 Carturan, L., Cazorzi, F., and Dalla Fontana, G.: Enhanced estimation of glacier mass  
657 balance in unsampled areas by means of topographic data, *Ann. Glaciol.*, 50, 37–46,  
658 2009.

659 Carturan, L., Baldassi, G., Bondesan, A., Calligaro, S., Carton, A., Cazorzi, F., Dalla  
660 Fontana, G., Francese, R., Guarnieri, A., Milan, N., Moro, D., Tarolli, P.: Current  
661 behavior and dynamics of the lowermost Italian glacier (Montasio Occidentale, Julian  
662 Alps), *Geografiska Annaler: Series A, Physical Geography*, 95, 79–96, 2013.

663 Carturan, L., Baroni, C., Carton, A., Cazorzi, F., Fontana, G. D., Delpero, C., and  
664 Zanoner, T.: Reconstructing Fluctuations of La Mare Glacier (Eastern Italian Alps) in  
665 the Late Holocene: new Evidence for a Little Ice Age Maximum Around 1600 AD.  
666 *Geografiska Annaler: Series A, Physical Geography*, 96, 287–306, 2014.

667 Carturan, L., Zuecco, G., Seppi, R., Zanoner, Z., Borga, M., Carton, A., and Dalla  
668 Fontana, G.: Catchment-scale permafrost mapping using spring water characteristics,  
669 *Permafrost Periglac.*, in press, doi: 10.1002/ppp.1875, 2015.

670 Chen, Y. and Medioni, G.: Object modeling by registration of multiple range images,  
671 in: *Proceedings, IEEE International Conference on Robotics and Automation*, 9–11  
672 April, Sacramento, CA, USA, 10, 145–155, 1991.

673 Dall’Asta, E., Delaloye, R., Diotri, F., Forlani, G., Fornari, M., Morra di Cella, U.,  
674 Pogliotti, P., Roncella, R., Santise, M.: Use of UAS in a high mountain landscape: the  
675 case of gran sommetta rock glacier (AO), *The International Archives of the*  
676 *Photogrammetry, Remote Sensing and Spatial Information Sciences*, Volume XL-  
677 3/W3, 391–397, 2015a.

678 Debella-Gilo, M. and Käab, A.: Sub-pixel precision image matching for measuring  
679 surface displacements on mass movements using normalized cross-correlation.  
680 *Remote Sens. Environ.*, 115, 130–142, 2011.

681 Favalli, M., Fornaciai, A., Isola, I., Tarquini, S., and Nannipieri, L.: Multiview 3D  
682 reconstruction in geosciences, *Comput. Geosci.*, 44, 168–176, 2012.

683 Gauthier, D., Conlan, M., and Jamieson, B.: Photogrammetry of fracture lines and  
684 avalanche terrain: potential applications to research and hazard mitigation projects,  
685 *Proceedings, International Snow Science Workshop, Banff*, 29 September–3 October  
686 2014, 109–115, 2014.

687 Glira, P., Pfeifer, N., Briese, C., Ressel, C.: A correspondence framework for ALS strip  
688 adjustments based on variants of the ICP algorithm, *Photogramm. Fernerkun.*, 4, 275–  
689 289, doi:10.1127/pfg/2015/0270, 2015.

690 Gómez-Gutiérrez, Á., de Sanjosé-Blasco, J. J., de Matías-Bejarano, J., and  
691 Berenguer-Sempere, F.: Comparing two photo-reconstruction methods to produce

692 high density point clouds and DEMs in the Corral del Veleta Rock Glacier (Sierra  
693 Nevada, Spain), *Remote Sensing*, 6, 5407–5427, 2014.

694 Gómez-Gutiérrez, Á., de Sanjosé-Blasco, J. J., Lozano-Parra, J., Berenguer-Sempere,  
695 F., and de Matías-Bejarano, J.: Does HDR pre-processing improve the accuracy of 3D  
696 models obtained by means of two conventional SfM-MVS software packages? The  
697 case of the Corral del Veleta Rock Glacier, *Remote Sensing*, 7, 10269–10294, 2015.

698 Hartley, R. and Zisserman, A.: *Multiple View Geometry*, In *Computer Vision*,  
699 Cambridge University Press, Cambridge, UK, 2003.

700 Haeberli, W.: Creep of mountain permafrost: internal structure and flow of alpine rock  
701 glaciers, *Mitteilungen der Versuchsanstalt für Wasserbau, Hydrologie und Glaziologie  
702 der ETH Zurich*, 77, 5–142, 1985.

703 Hosseinaveh, A., Sargeant, B., Erfani, T., Robson, S., Shortis, M., Hess, M., and  
704 Boehm, J.: Towards fully automatic reliable 3D acquisition: from designing imaging  
705 network to a complete and accurate point cloud, *Robotics and Autonomous Systems*,  
706 62, 1197–1207, 2014.

707 Huss, M.: Density assumptions for converting geodetic glacier volume change to mass  
708 change, *The Cryosphere*, 7, 877-887, doi:10.5194/tc-7-877-2013, 2013.

709 Immerzeel, W. W., Kraaijenbrink, P. D. A., Shea, J. M., Shrestha, A. B., Pellicciotti, F.,  
710 Bierkens, M. F. P., and De Jong, S. M.: High-resolution monitoring of Himalayan glacier  
711 dynamics using unmanned aerial vehicles, *Remote Sens. Environ.*, 150, 93–103,  
712 2014.

713 Isaksen, K., Ødegård, R. S., Eiken, T., and Sollid, J. L.: Composition, flow and  
714 development of two tongue-shaped rock glaciers in the permafrost of Svalbard.  
715 *Permafrost and Periglacial Processes*, 11, 241-257, 2000.

716 James, M. R. and Robson, S.: Straightforward reconstruction of 3D surfaces and  
717 topography with a camera: accuracy and geoscience application, *J. Geophys. Res.-  
718 Earth*, 117, F03017, doi:10.1029/2011JF002289, 2012.

719 James, M. R. and Robson, S.: Mitigating systematic error in topographic models  
720 derived from UAV and ground-based image networks, *Earth Surf. Proc. Land.* 39,  
721 1413–1420, doi:10.1002/esp.3609, 2014.

722 Kääb, A.: Monitoring high-mountain terrain deformation from repeated air-and  
723 spaceborne optical data: examples using digital aerial imagery and ASTER data.  
724 ISPRS Journal of Photogrammetry and remote sensing, 57, 39–52, 2002.

725 Kääb, A.: Remote Sensing of Mountain Glaciers and Permafrost Creep. Research  
726 Perspectives from Earth Observation Technologies and Geoinformatics, Schriftenreihe  
727 Physische Geographie, Glaziologie und Geomorphodynamik, 48, University of Zurich,  
728 Zurich, Switzerland, 2005.

729 Kääb, A., Kaufmann, V., Ladstädter, R., and Eiken, T.: Rock glacier dynamics:  
730 implications from high-resolution measurements of surface velocity fields, in: Eighth  
731 International Conference on Permafrost, 21–25 July 2003, Zurich, Switzerland, Vol. 1,  
732 501–506, 2003.

733 Kääb, A., Girod, L., and Berthling, I.: Surface kinematics of periglacial sorted circles  
734 using structure-from-motion technology, The Cryosphere, 8, 1041–1056,  
735 doi:10.5194/tc-8-1041-2014, 2014.

736 Micheletti, N., Chandler, J. H., and Lane, S. N.: Investigating the geomorphological  
737 potential of freely available and accessible Structure-from-Motion photogrammetry  
738 using a smartphone, Earth Surf. Proc. Land., 40, 473–486, doi:10.1002/esp.3648,  
739 2014.

740 Nilosek, D., Sun, S., and Salvaggio, C.: Geo-accurate model extraction from three-  
741 dimensional image-derived point clouds, in: Proceedings of SPIE, Algorithms and  
742 Technologies for Multispectral, Hyperspectral, and Ultraspectral Imagery XVIII, 23 April  
743 2012, Baltimore, MD, USA, 8390, 83900J, doi:10.1117/12.919148, 2012.

744 Nocerino, E., Menna, F., and Remondino, F.: Accuracy of typical photogrammetric  
745 networks in cultural heritage 3D modeling projects, ISPRS-International Archives of  
746 the Photogrammetry, Remote Sensing and Spatial Information Sciences, 1, 465–472,  
747 2014.

748 [Østrem, G. and Brugman, M.: Glacier mass-balance measurements: A manual for field](#)  
749 [and office work, NHRI Science Report, Saskatoon, Canada, 224 pp., 1991.](#)

750 Piermattei, L., Carturan, L., and Guarnieri, A.: Use of terrestrial photogrammetry based  
751 on structure from motion for mass balance estimation of a small glacier in the Italian  
752 Alps, *Earth Surf. Proc. Land.*, 40, 1791–1802, doi:10.1002/esp.3756, 2015.

753 Ryan, J. C., Hubbard, A. L., Box, J. E., Todd, J., Christoffersen, P., Carr, J. R., Holt, T.  
754 O., and Snooke, N.: UAV photogrammetry and structure from motion to assess calving  
755 dynamics at Store Glacier, a large outlet draining the Greenland ice sheet, *The*  
756 *Cryosphere*, 9, 1–11, doi:10.5194/tc-9-1-2015, 2015.

757 Roer, I. and Nyenhuis, M.: Rockglacier activity studies on a regional scale: comparison  
758 of geomorphological mapping and photogrammetric monitoring, *Earth Surf. Proc.*  
759 *Land.*, 32, 1747–1758, 2007.

760 [Rolstad, C., Haug, T. and Denby, B.: Spatially integrated geodetic glacier mass](#)  
761 [balance and its uncertainty based on geostatistical analysis: Application to the western](#)  
762 [Svartisen ice cap, Norway. \*J. Glaciol.\*, 55\(192\), 666-680, doi:](#)  
763 [10.3189/002214309789470950, 2009.](#)

764 Seppi, R., Carton, A., Zumiani, M., Dall’Amico, M., Zampedri, G., and Rigon, R.:  
765 Inventory, distribution and topographic features of rock glaciers in the southern region  
766 of the Eastern Italian Alps (Trentino). *Geografia Fisica e Dinamica Quaternaria* 35,  
767 185–197, doi:10.4461/GFDQ.2012.35.17, 2012.

768 Solbø, S. and Storvold, R.: Mapping svalbard glaciers with the cryowing uas, *ISPRS*  
769 *International Archives of the Photogrammetry, Remote Sensing and Spatial*  
770 *Information Sciences*, XL-1/W2, 373–377, 2013.

771 Tonkin, T. N., Midgley, N. G., Graham, D. J., and Labadz, J. C.: The potential of small  
772 unmanned aircraft systems and structure-from-motion for topographic surveys: a test  
773 of emerging integrated approaches at Cwm Idwal, North Wales, *Geomorphology*, 226,  
774 35–43, 2014.

775 [Triggs, B., McLauchlan, P. F., Hartley, R. I., and Fitzgibbon, A. W.: Bundle adjustment](#)  
776 [– A modern synthesis, in: \*Vision algorithms: theory and practice\*. Springer Berlin](#)  
777 [Heidelberg, 298-372, 1999.](#)

778 Tseng, C.-M., Lin, C. W., Dalla Fontana, G., [and](#) Tarolli, P.: The topographic signature  
779 of a Major Typhoon, *Earth Surf. Proc. Land.*, 40, 1129–1136, 2015.

780 Verhoeven, G., Karel, W., 'tuhec, S., Doneus, M., Trinks, I., and Pfeifer, N.: Mind your  
781 grey tones – examining the influence of decolourization methods on interest point  
782 extraction and matching for architectural image-based modelling, in: 3D-Arch 2015–  
783 3D Virtual Reconstruction and Visualization of Complex Architectures (ISPRS WG V/4,  
784 CIPA), 25–27 February 2015, Vol. 40, ISPRS, Avila, Spain, 307–314, 2015.

785 [Zemp, M., Thibert, E., Huss, M., Stumm, D., Rolstad Denby, C., Nuth, C., Nussbaumer,](#)  
786 [S.U., Moholdt, G., Mercer, A., Mayer, C., Joerg, P.C., Jansson, P., Hynek, B., Fischer,](#)  
787 [A., Escher-Vetter, H., Elvehøy, H. and Andreassen, L.M.: Reanalysing glacier mass](#)  
788 [balance measurement series. The Cryosphere, 7, 1227-1245, doi:10.5194/tc-7-1227-](#)  
789 [2013, 2013.](#)

790 Wackrow, R. and Chandler, J.: Minimising systematic error surfaces in digital elevation  
791 models using oblique convergent imagery, Photogramm. Rec., 26, 16–31, 2011.

792 Wenzel, K., Rothermel, M., Fritsch, D., and Haala, N.: Image acquisition and model  
793 selection for multi-view stereo, Int. Arch. Photogramm. Remote Sens. Spatial Inf. Sci,  
794 251–258, 2013.

795 Whitehead, K., Moorman, B. J., and Hugenholtz, C. H.: Brief Communication: Low-  
796 cost, ondemand aerial photogrammetry for glaciological measurement, The  
797 Cryosphere, 7, 1879–1884, doi:10.5194/tc-7-1879-2013, 2013.

798 Zemp, M., Thibert, E., Huss, M., Stumm, D., Denby, C. R., Nuth, C., Nussbaumer, S.  
799 U., Moholdt, G., Mercer, A., Mayer, C., Joerg, P. C., Jansson, P., Hynek, B., Fischer,  
800 A., Escher-Vetter, H., Elvehøy, H., and Andreassen, L. M.: Reanalysing glacier mass  
801 balance measurement series. The Cryosphere, 7, 1227-1245, doi:10.5194/tc-7-1227-  
802 2013, 2013.

803

804

805

806

807

808

809

810

811

|812

813 **Table 1.** Date and main parameters of available LiDAR data. The dash indicates no  
 814 available information.

Date	Aircraft	Laser scanner model	Laser scanner rate	Max. scan angle	Scan frequency	Point density [pts·m <sup>-2</sup> ]
24 Sept. 2014	Helicopter AS350 B3	Optech ALTM GEMINI (04SEN164)	100 kHz	46°	34 Hz	5.1
22 Sept. 2013	Cessna 404 D-IDOS	ALTM 3100	70,000 Hz	±25°	32 Hz	0.9
17 Sept. 2003	—	—	—	—	—	0.5

815

816 **Table 2.** Data acquisition settings and processing results of the photogrammetric  
 817 surveys for both case studies. The GCPs error is the average transformation residuals  
 818 error [m] and root mean square reprojection error for the GCPs [pix] during the bundle  
 819 adjustment computation. The image quality refers to the downsampling represents the  
 820 downsized of the images resolution during the dense matching computation. “Ultra  
 821 high” means full resolution, “High” a downsized-downsampling of 50% before the image  
 822 matching procedure. The ground sample distance (GSD) is the average pixel  
 823 size on the ground. The standard deviation of the ICP (Iterative Closest Point)  
 824 registration is reported in the table.

	La Mare glacier		Rock glacier
	4 September 2013	27 September 2014	27 September 2014
<i>Input data</i>			
Camera type	Nikon 600D	Nikon 600D	Canon 5D Mark III
Focal Length	25 mm	35 mm	28 mm
Image size	5184 x 3456 pix	5184 x 3456 pix	5760 x 3840 pix
N° Images	37	177	198
<u>Acquisition time</u>	<u>10:10 – 12:00</u>	<u>7:50 – 10:40</u>	<u>12:15 – 14:00</u>
<i>Processing data</i>			
Reprojection error	0.43 pix (1.76 max)	0.40 pix (3.75 max)	0.38 pix (1.20 max)
GCPs error	1.52 m 1.48 pix	1.14 m 1.96 pix	0.62 m 1.86 pix
Image quality	Ultra high	High	High
Mean GSD	0.16 m/pix	0.22 m/pix	0.064 m/pix
Dense point cloud	49,844,094 pts	55,114,074 pts	56,171,705 pts
Point density	37 pts m <sup>-2</sup>	20 pts m <sup>-2</sup>	244 pts m <sup>-2</sup>
<i>Post-processing data</i>			
Filtered point cloud /subsampled	15,617,342 pts (sampled 0.20 m)	24,226,221 pts (sampled 0.20 m)	4,517,143 pts (sampled 0.10 m)
Point density	8 pts m <sup>-2</sup>	9 pts m <sup>-2</sup>	21 pts m <sup>-2</sup>
ICP transformation	0.14 m	0.15 m	0.10 m

825

826 **Table 3.** ~~Results of Comparisons~~ between SfM-MVS-based DEMs and vs. ALS-  
 827 based DEMs in the common area outside and inside the La Mare Glacier. ~~and for the~~  
 828 ~~bare-ground stable area and glacier.~~

Elevation differences [m] cell size 1 m x 1m								
DEMs	Common SfM-MVS bare-ground area				Common SfM-MVS glacier area			
	<i>Min</i>	<i>Max</i>	<i>Mean</i>	$\sigma$	<i>Min</i>	<i>Max</i>	<i>Mean</i>	$\sigma$
SfM-MVS - ALS 2013 2013	-19.59	33.61	-0.42	1.72	-9.91	12.04	-0.13	0.78
SfM-MVS - ALS 2014 2014	-18.48	22.42	0.03	0.74	-18.17	11.41	0.23	0.65
SfM-MVS - SfM-MVS 2014 2013	-33.12	14.19	0.38	1.73	-12.44	12.33	1.58	1.42
ALS 2014 - ALS 2013	-15.38	10.81	-0.09	0.29	-14.61	7.37	1.30	0.97

829

830 **Table 4.** Mass balance calculations on La Mare Glacier~~s~~ using different combinations  
 831 of SfM-MVS and ALS DEMs.

Mass balance estimation								
DEMs cell size 10 m	Spatial coverage [m <sup>2</sup> ]	Average elevation changes [m]		Volume change [m <sup>3</sup> ]		Mass balance [m w.e]		
		<i>Raw</i>	<i>Corrected</i>	<i>Raw</i>	<i>Corrected</i>	<i>Raw</i>	<i>Corrected</i>	
SfM-MVS - SfM-MVS 2014 2013	1,834,800	1.81	1.45	3,320,988	2,660,460	1.09	0.87 <u>± 1.30</u>	
ALS 2014 - ALS 2013	(~88%)	1.47	1.56	2,697,156	2,862,288	0.88	0.94 <u>± 0.16</u>	
SfM-MVS - ALS 2013 2014	1,938,700	1.64	1.70	3,179,468	3,295,790	0.98	1.02 <u>± 0.60</u>	
ALS 2014 - ALS 2013	(~93%)	1.41	1.50	2,733,567	2,908,050	0.85	0.90 <u>± 0.16</u>	
ALS 2014 - ALS 2013	2,072,700 (entire glacier)	1.43	1.52	2,963,961	3,150,504	0.86	0.91 <u>± 0.16</u>	

832

833

834

835

836

837

838

839

840

841

842 **Table 5.** Statistics of elevation changes in the rock glacier and in bare ground stable  
843 area ~~off~~-outside the rock glacier from September 2014 to September 2013 and  
844 September 2003 in the ALS reconstructed area and in the common ALS and SfM-MVS  
845 coverage area.

<i>DEMsata</i>		Elevation changes [m]							
		ALS Reconstructed area				SfM-MVS Reconstructed area			
		Stable area		Rock glacier		Stable area		Rock glacier	
		<i>Mean</i>	$\sigma$	<i>Mean</i>	$\sigma$	<i>Mean</i>	$\sigma$	<i>Mean</i>	$\sigma$
SfM-MVS 2014	- ALS 2014	—	—	—	—	0.05	0.31	0.02	0.17
SfM-MVS 2014	- ALS 2013	—	—	—	—	0.01	0.33	-0.04	0.18
ALS 2014	- ALS 2013	-0.05	0.19	-0.07	0.12	-0.05	0.20	-0.07	0.12
SfM-MVS 2014	- ALS 2003	—	—	—	—	0.06	0.33	-0.16	0.49
ALS 2014	- ALS 2003	-0.01	0.22	-0.18	0.46	-0.00	0.21	-0.18	0.47
ALS 2013	- ALS 2003	0.04	0.21	-0.11	0.41	—	—	—	—

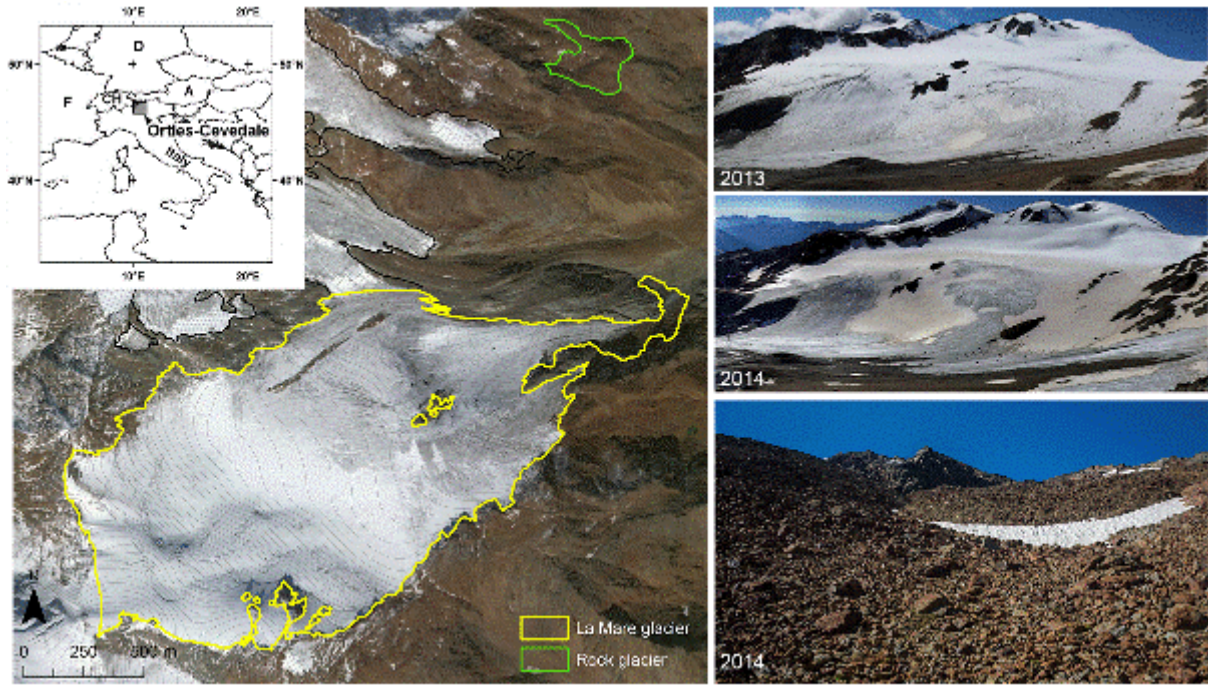
846

847 **Table 6.** Velocity statistics in three distinct areas of the rock glacier and in stable area  
848 outside the rock glacier evaluated comparing the 2003 and 2014 ALS DEMs and the  
849 photogrammetric DEM for the 2014 survey epoch.

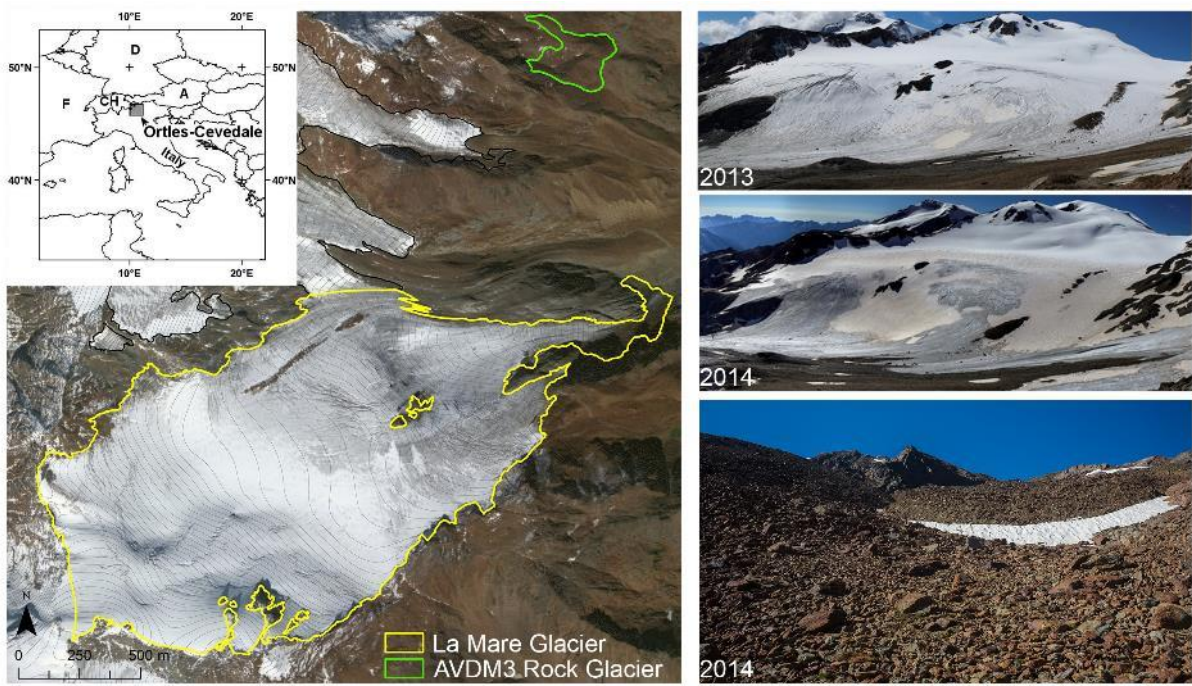
Horizontal movements between 2003 and 2014 [cm yr <sup>-1</sup> ]										
	ALS 2003 - ALS 2014					ALS 2003 - SfM-MVS 2014				
	<i>No. points</i>	<i>Min</i>	<i>Max</i>	<i>Mean</i>	$\sigma$	<i>No. points</i>	<i>Min</i>	<i>Max</i>	<i>Mean</i>	$\sigma$
Area 1	41	7.3	43.3	26.8	8.9	36	6.8	47.5	26.3	10.3
Area 2	13	4.4	27.4	18.9	7.0	11	9.0	27.9	18.1	6.4
Area 3	26	4.5	16.5	9.4	4.0	24	4.5	18.2	9.0	4.1
Off rock glacier	65	0.0	10.7	3.6	3.1	23	0.0	13.6	5.3	4.2

850

851



852

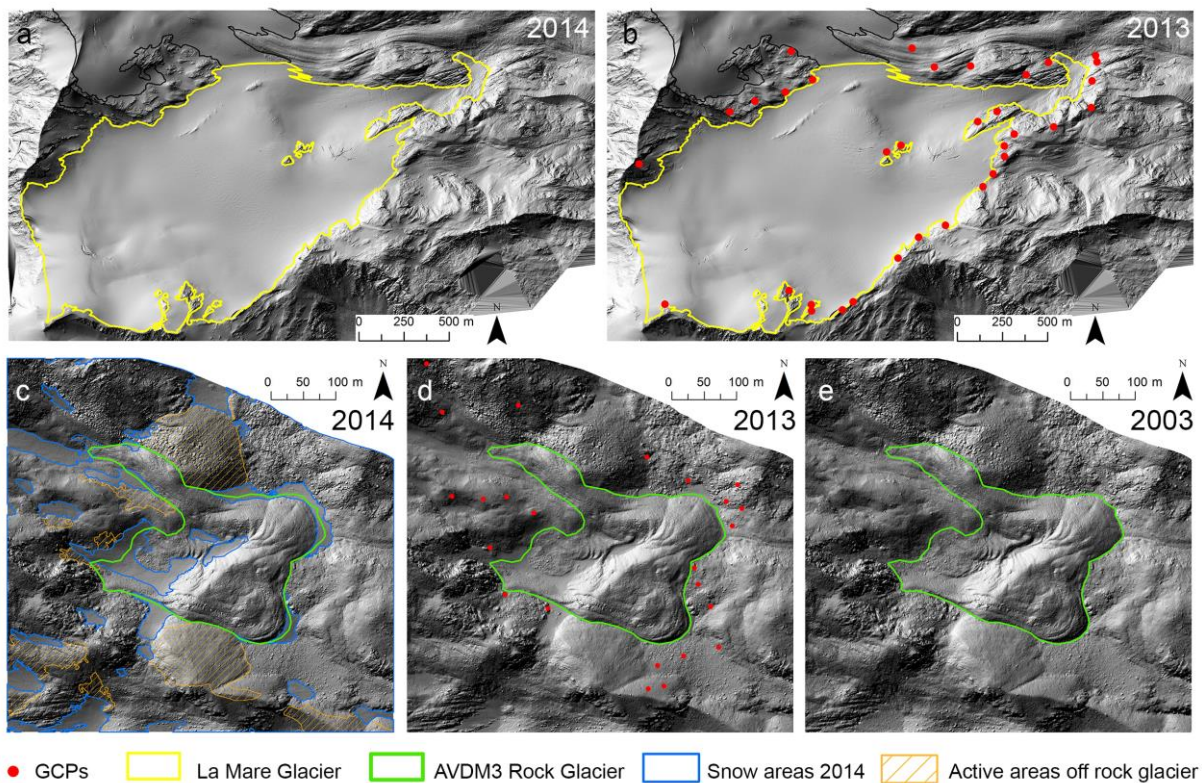
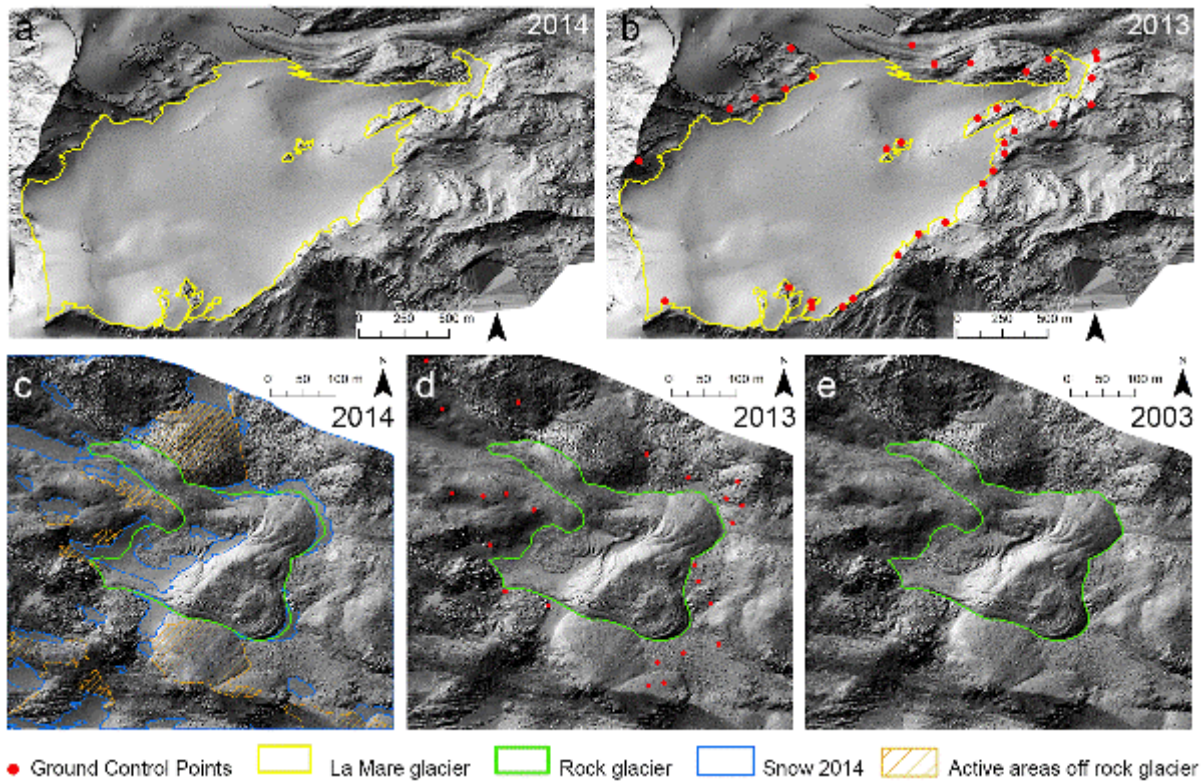


853

854 **Figure 1.** Geographic setting of study areas. Panoramica view of the La Mare Glacier  
 855 from the same camera position on 4 September 2013 and 27 September 2014. The  
 856 lower right photograph shows the front of the meridional lobe of the AVDM3 Rock  
 857 Glacier, which was surveyed on 27 September 2014.

858

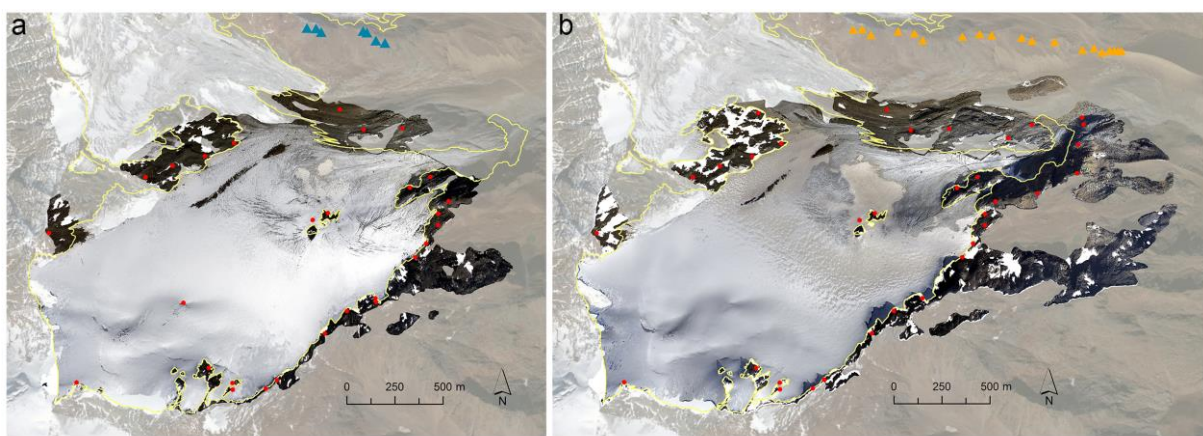
859



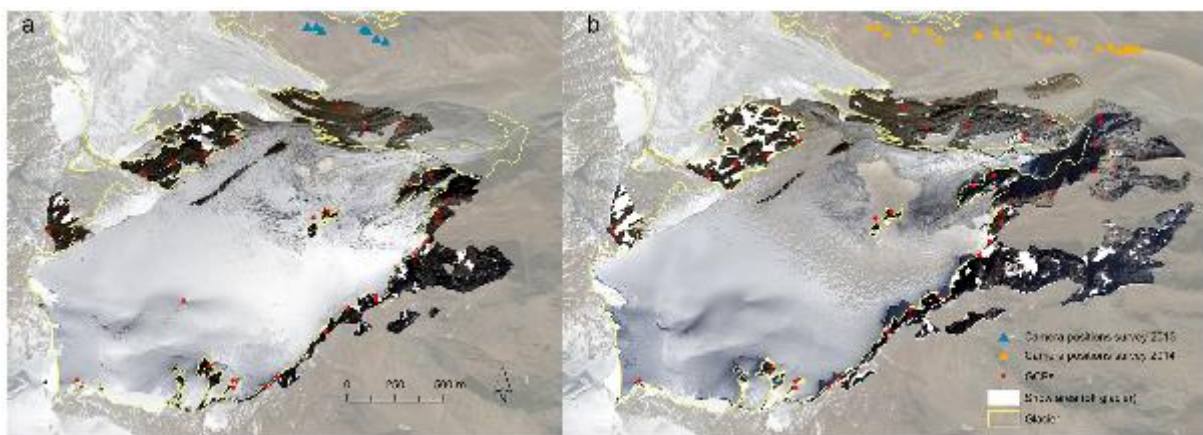
862 **Figure 2.** ALS Hillshade of the ALS DEMs of La Mare glacier acquired on (a)  
 863 September 24, 2014 and (b) September 21, 2013. The Hillshades of the ALS DEMs of  
 864 rock glacier acquired on (c) 2014, (d) 2013 and (e) 2003. The red dots represent the  
 865 selected GCPs in 2013 DEM used for the photogrammetric approach. The snow

866 accumulation areas and the geomorphologically-active areas outside the rock glacier  
 867 were excluded during the ICP computation between 2013 and 2003, 2014 ALS point  
 868 cloud.

869  
 870  
 871  
 872

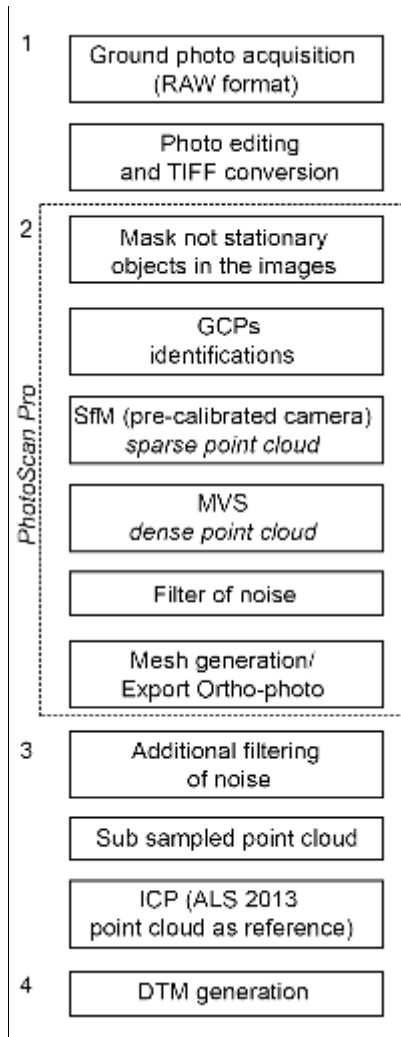


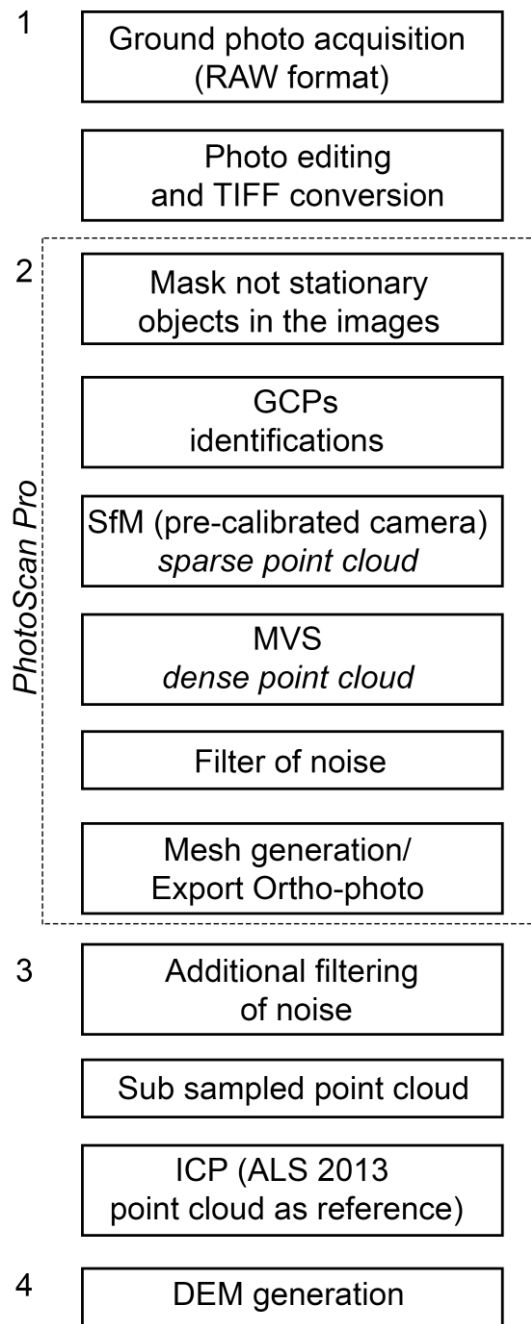
873 ● GCPs ▲ Camera position survey 2013 ▲ Camera position survey 2014 □ La Mare Glacier □ Snow areas (off glacier)



874

875 **Figure 3.** Orthophotos derived from the images of SfM-MVS 3D model of La Mare  
 876 Glacier surveyed on (a) 4 September 2013 and (b) 27 September 2014. The white  
 877 areas in the ortho-images represent the snow-covered area in the rock stable area.  
 878 The red dots outside the glacier area are the GCPs and the triangles are the identified  
 879 the camera locations.

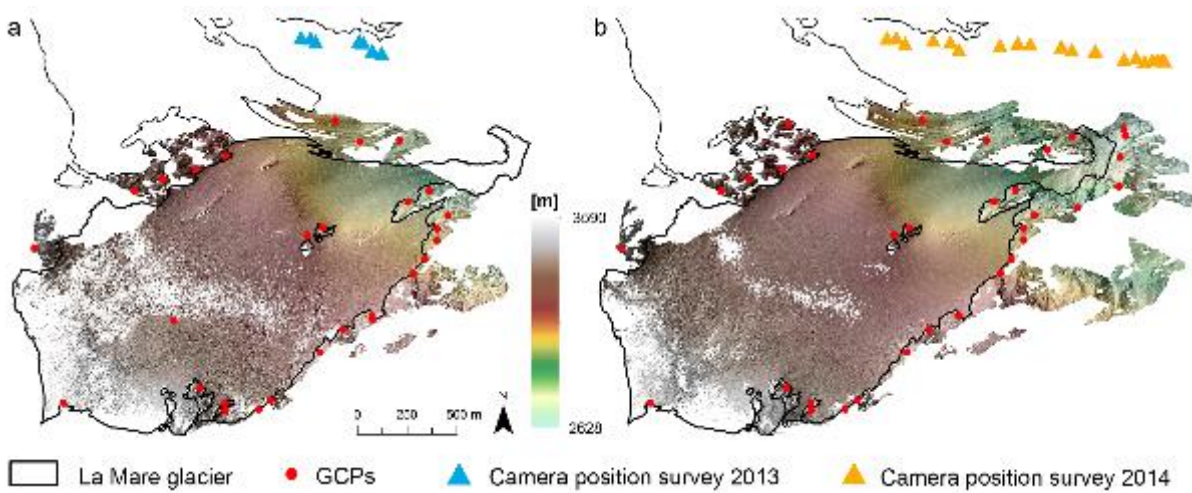




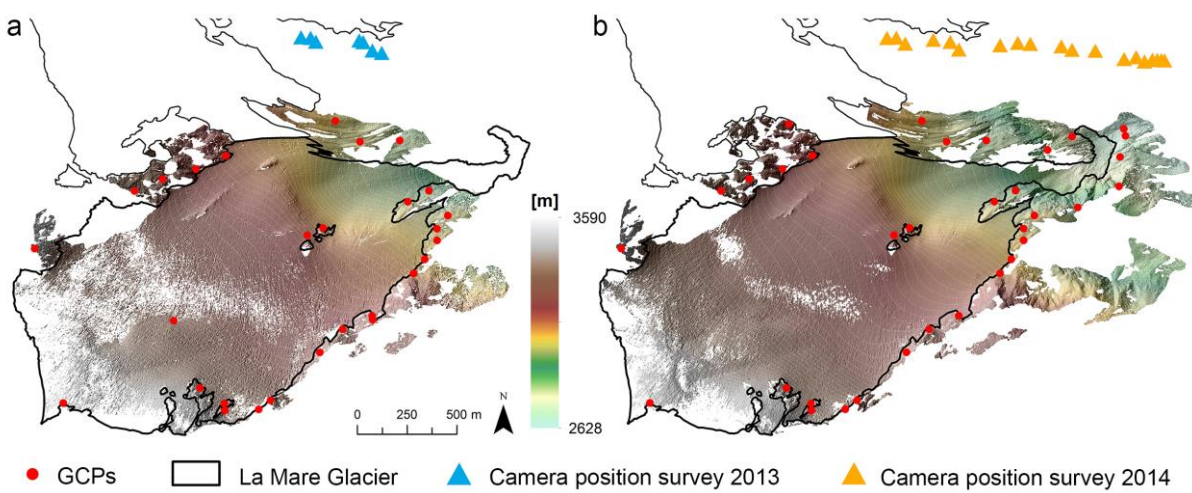
881

882 **Figure 4.** Workflow illustrating the photo-based 3D reconstruction process used in this  
 883 work for both case studies, starting from images collection through the DEM  
 884 generation.

885



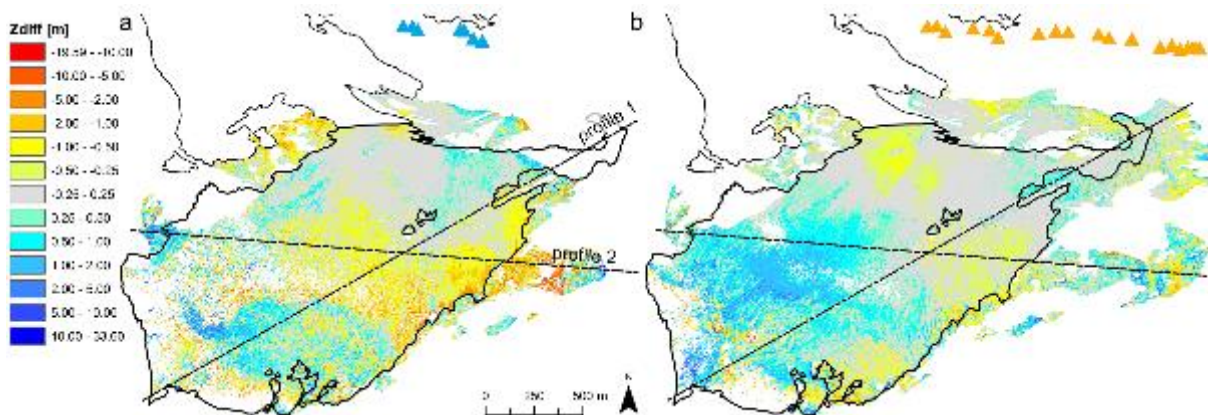
886



887

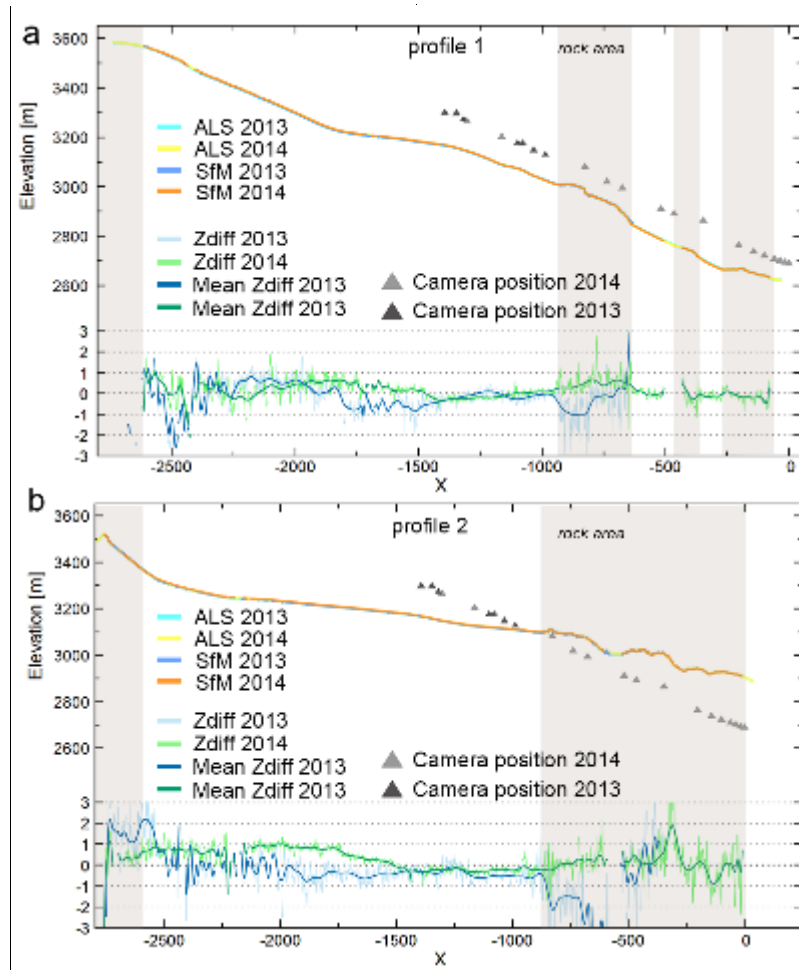
888 **Figure 5.** Hillshaded DEMs with superposed semi-transparent colour-map of La Mare  
 889 Glacier derived from photogrammetric measurements for **(a)** 4 September 2013  
 890 and **(b)** 27 September 2014 image surveys.

891

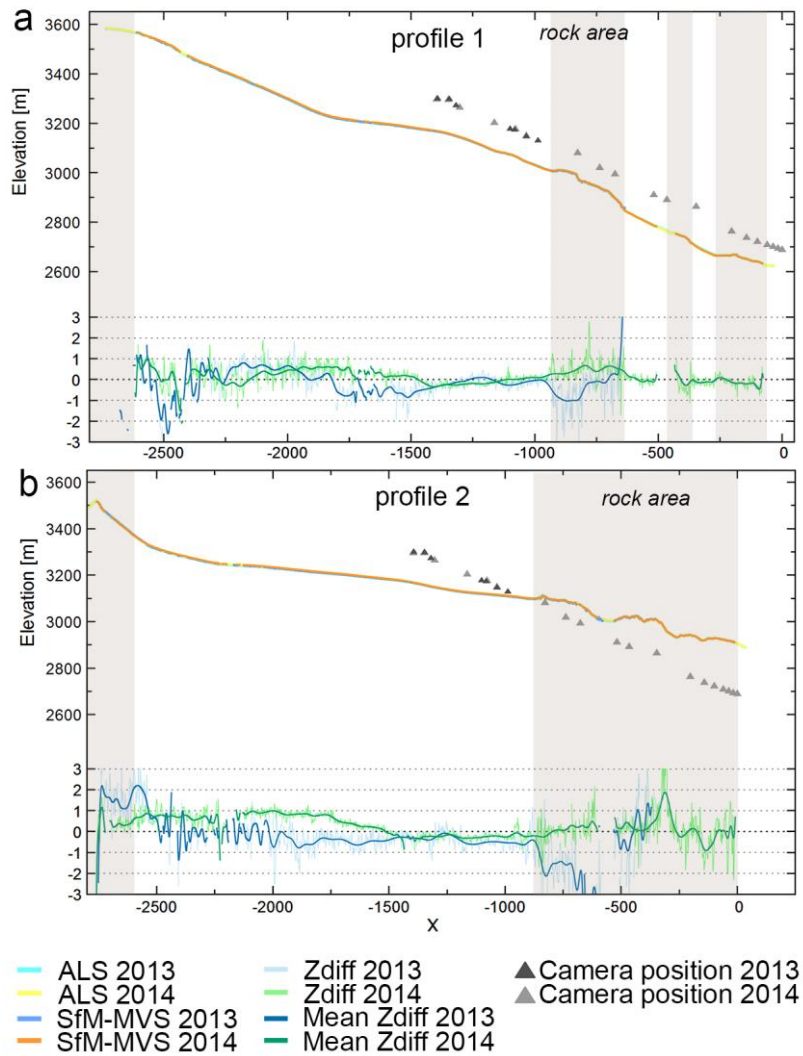


892

893 **Figure 6.** Spatial distribution of elevation differences between photogrammetric and  
 894 ALS-based DEMs **for** **(a)** 2013 and **(b)** 2014. Black lines are the location of profiles  
 895 in Fig. 7.  
 896



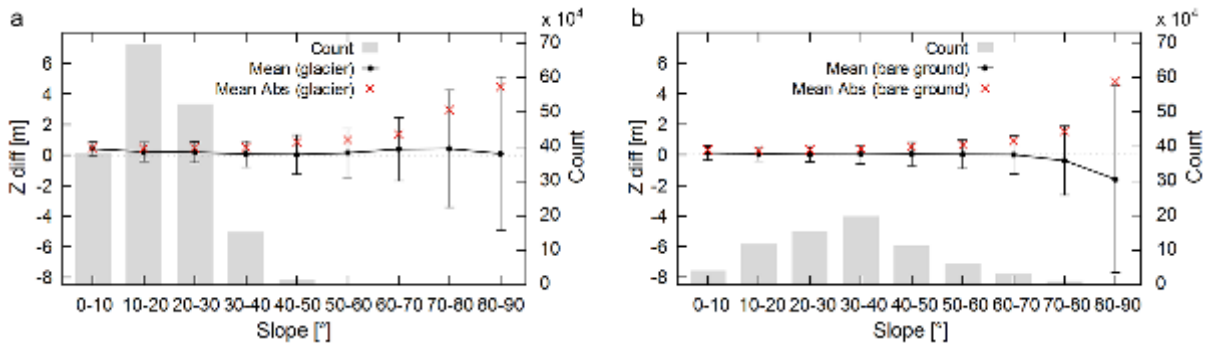
897



898

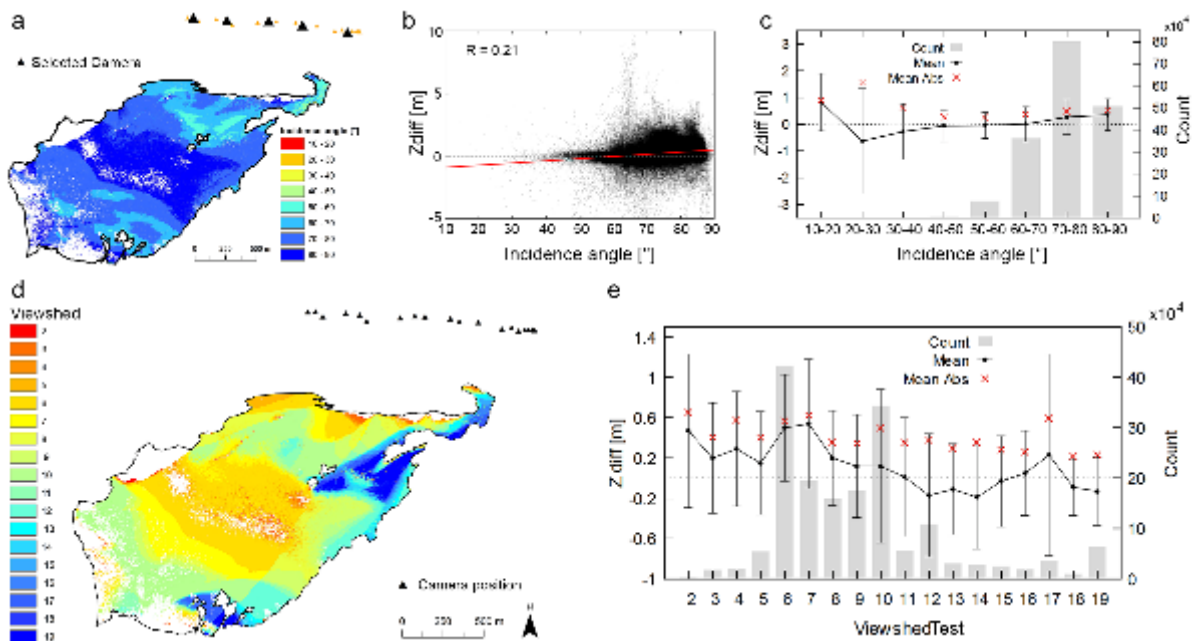
899 **Figure 7.** Cross sections through the La Mare Glacier DEMs show the glacier  
 900 elevation change and the difference between 2013 and 2014 in SfM-MVS and ALS-  
 901 based DEMs. The location of **(a)** ~~the~~ profile 1 and **(b)** profile 2 is indicated in Fig. 6.  
 902 The x-axis zero has been fixed at the first camera position of the 2014 survey and the  
 903 minimum and maximum values of the z-difference set to  $\pm 3$  m and both profiles and  
 904 the camera positions were projected onto the xz-plane. The shaded area represent bare  
 905 ground stable areas.

906

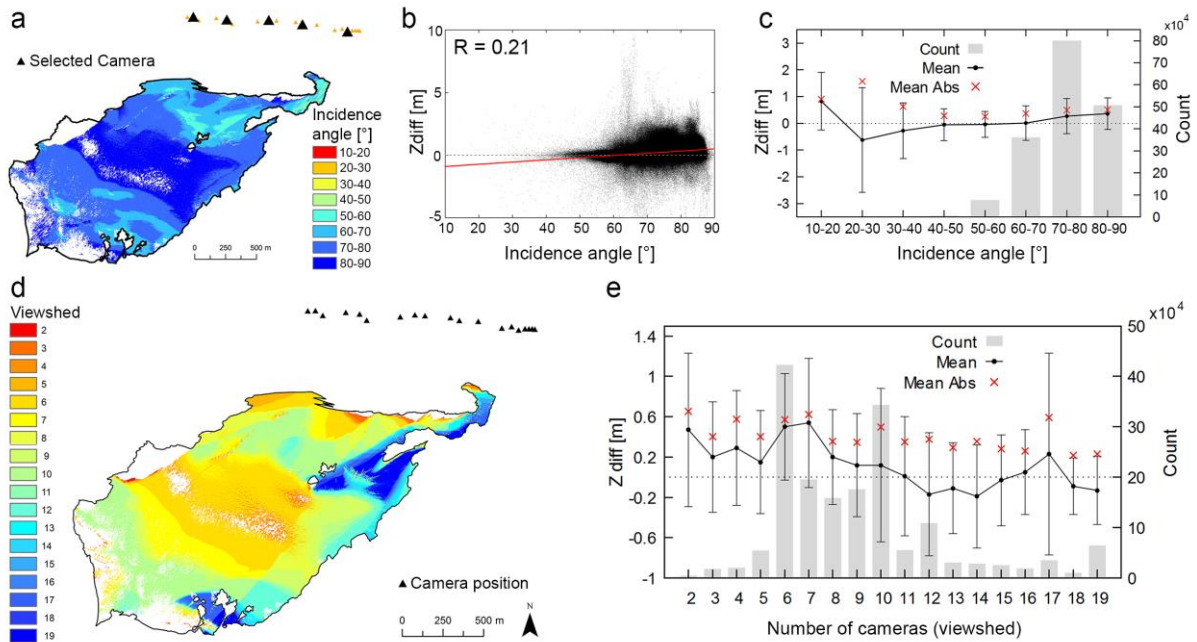


907

908 **Figure 8.** Mean, mean of the absolute values and standard deviation of the 2014 DoD  
 909 between SfM-MVS and ALS-based DEM depending on slope calculated (a) inside  
 910 glacier area and (b) in the bare ground outside glacier covered by rock. The grey bars  
 911 show the count of cells at any given slope (y-axis on the right).



912



913

914

915

916

917

918

919

920

921

922

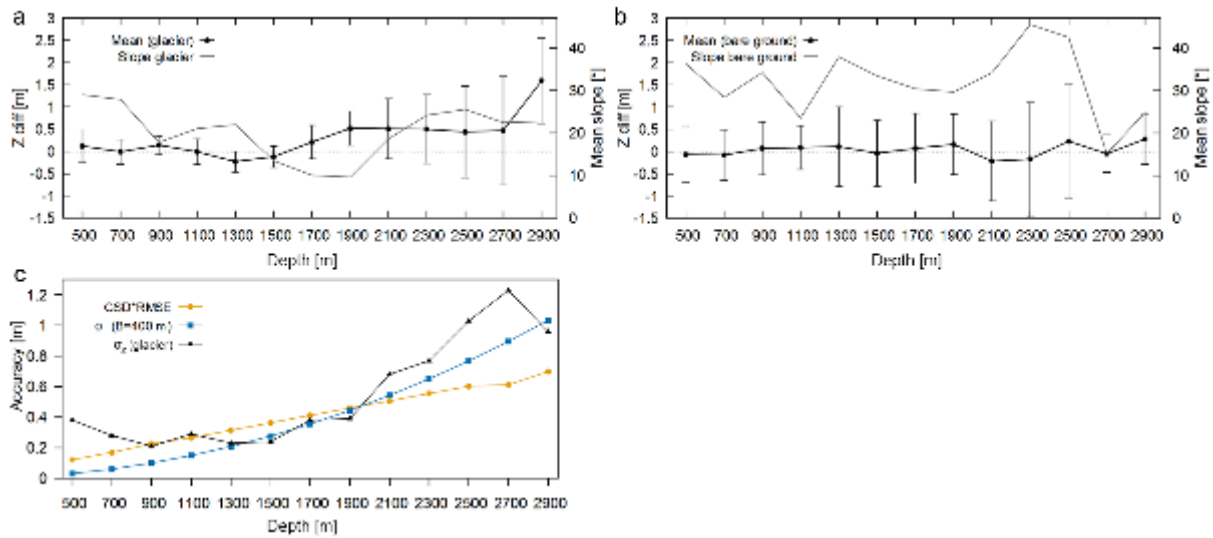
923

924

925

**Figure 9.** Mean incidence angles between five representative cameras positions and vectors normal to the surface and viewshed analysis. **(a)** Map of the mean incidence angle calculated for five representative camera positions; **(b)** the scatterplot of the elevation difference and the mean incidence angle for the five representative camera positions; **(c)** mean with one standard deviation error bars in y and mean of the absolute value of elevation differences for the mean incidence angle intervals calculated for the 5 selected representative camera positions, in 10 degree bins; **(d)** map of the analysis using viewshed number of cameras able to see each pixel derived from reconstructed area visible from all camera positions; **(e)** mean with one standard deviation y-error bars and mean of the absolute value of elevation differences for the viewshed reconstructed area analysis.

926



927

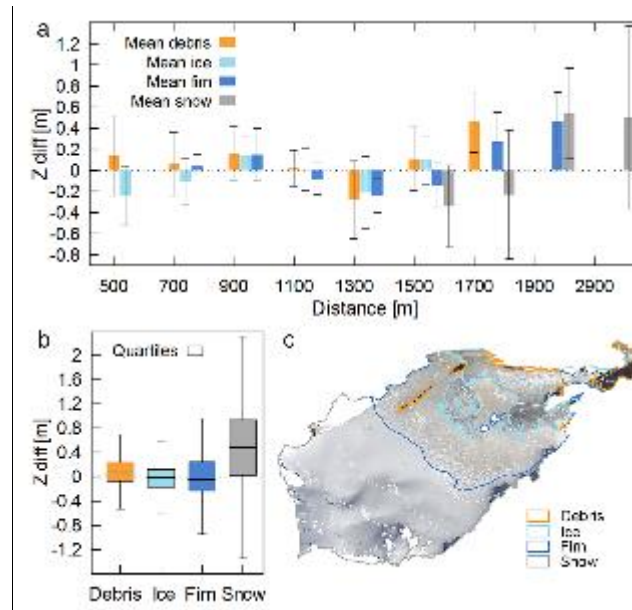
928 **Figure 10.** Mean and standard deviation of the 2014 DoD between SfM-MVS and ALS-  
929 based DEM depending on the distance from the camera depth calculated **(a)** with in the  
930 glacier area and **(b)** in the bare ground outside the glacier covered by rock. The trend  
931 of the average slope angle for each depth intervals is shown on the right y-axis. **(c)**  
932 Comparison of  $\sigma_z$  measured with in the glacier-reconstructed area, the theoretical depth  
933 accuracy estimated according to the-Eq. (1) and the GSD multiplied byfor the GCPs  
934 RMSE for eachthe depth intervals.

935

936

937

938



939

940

941

942

943

944

945

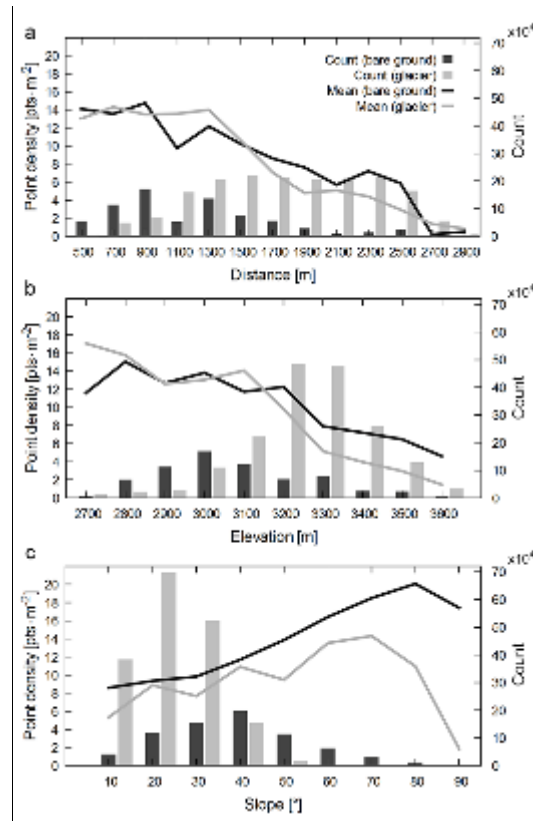
946

947

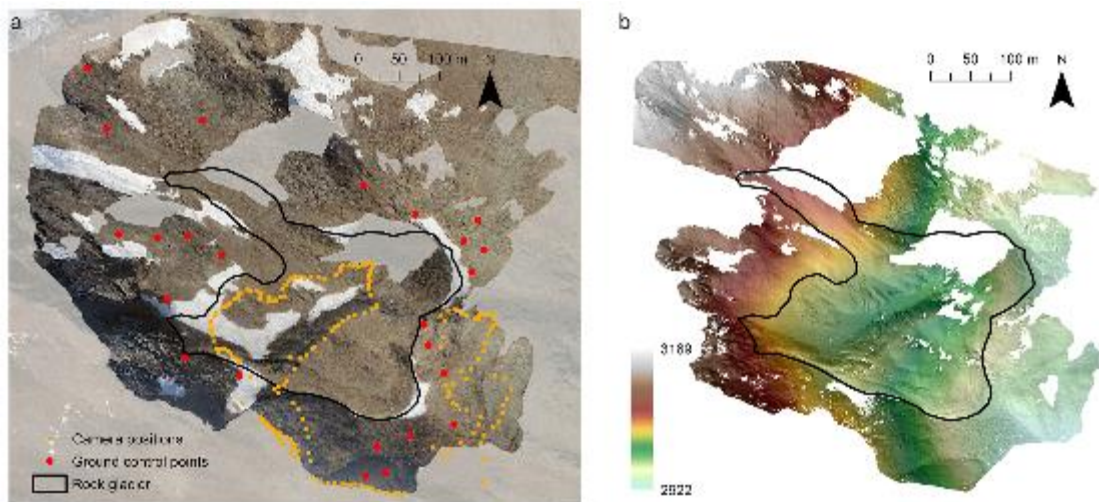
**Figure 11.** Elevation difference between the 2014 SfM-MVS and ALS-based DEMs calculated for different substrata. The figure shows **(a)** the mean and standard deviation of z-difference for four substrata (debris, ice, firn, and snow) grouped by distance from camera position; **(b)** the box plot of the z-difference for four substrata. In the box-whisker plot, values which exceed  $1.5 * IQR$  were considered outliers. In panel **(c)** the orthophoto of the glacier on 27 September 2014 and map of substrata.

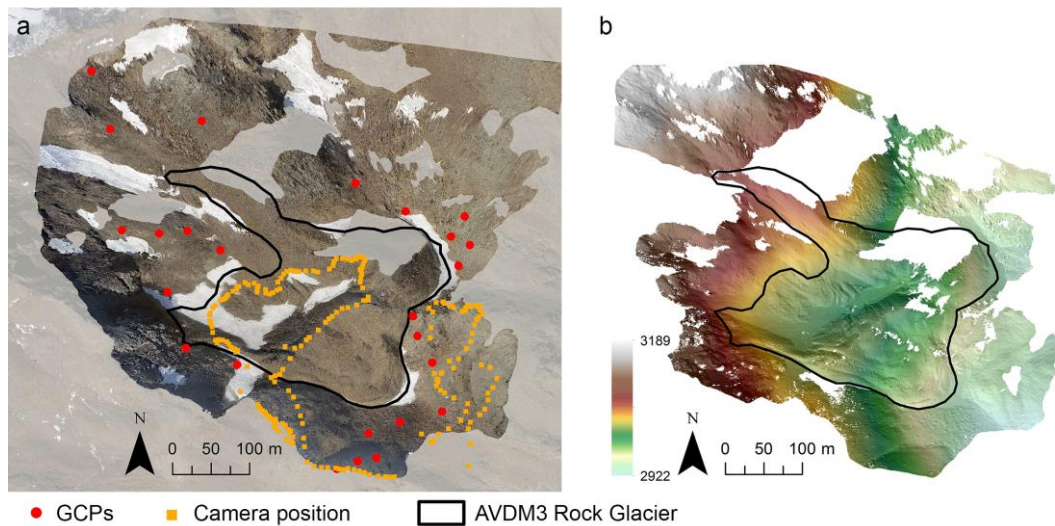
948

949 **Figure 12.** Relationships between point density of the 2014 photogrammetric 3D  
950 model and **(a)** camera-object distance, **(b)** elevation and **(c)** slope calculated for the  
951 glacier and rock stable area outside glacier. The point density was estimated using the  
952 filtered and subsampled point cloud.



953

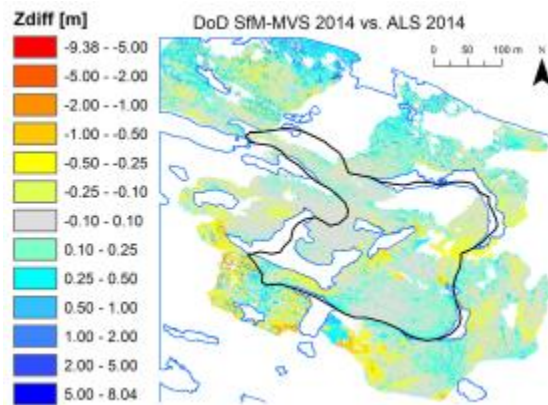




954

955 **Figure 13.** Correspondence between (a) the orthophoto of SfM-MVS 3D model of rock  
 956 glacier surveyed on 27 September 2014 and (b) the hillshade model overlain on colour-  
 957 coded elevations of the rock glacier ~~model-DEM~~ calculated at using the same data ~~and~~  
 958 ~~hour of the images acquisition~~. The holes in the DEM represent not are areas not  
 959 reconstructed-area.

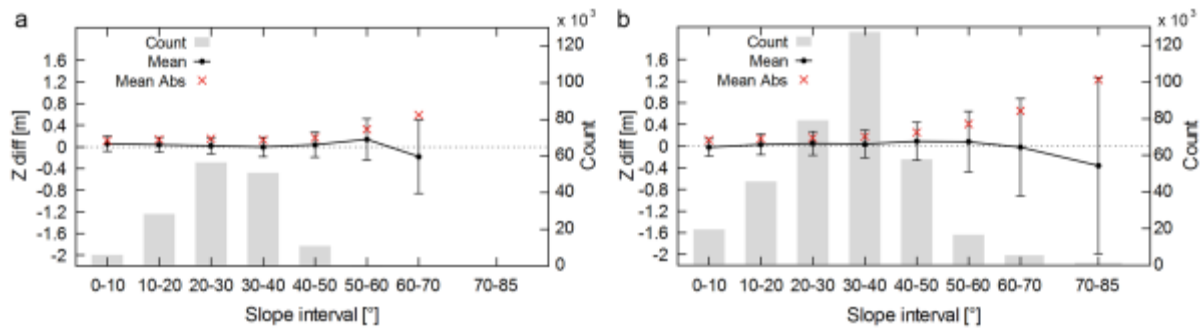
960



961

962 **Figure 14.** Spatial distribution of elevation differences between photogrammetric and  
 963 ALS-based DEM acquired on 27 September 2014 and 24 September 2014,  
 964 respectively. The blue shape-outline is the snow accumulation areas which were  
 965 excluded during the DEMs comparison.

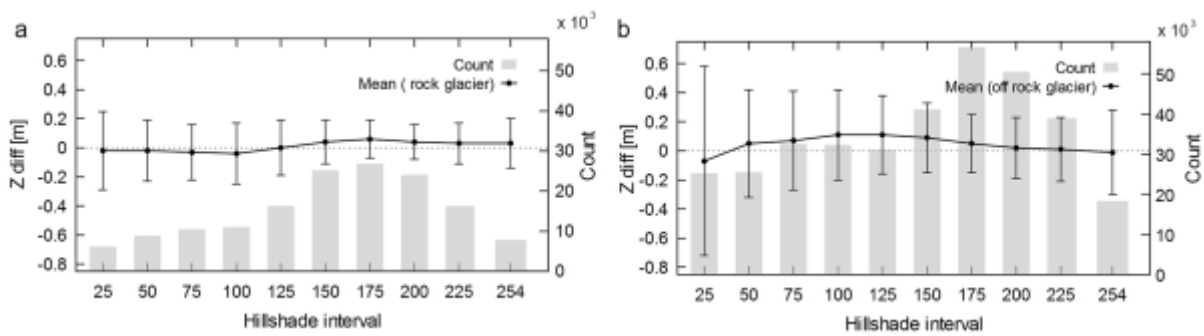
966



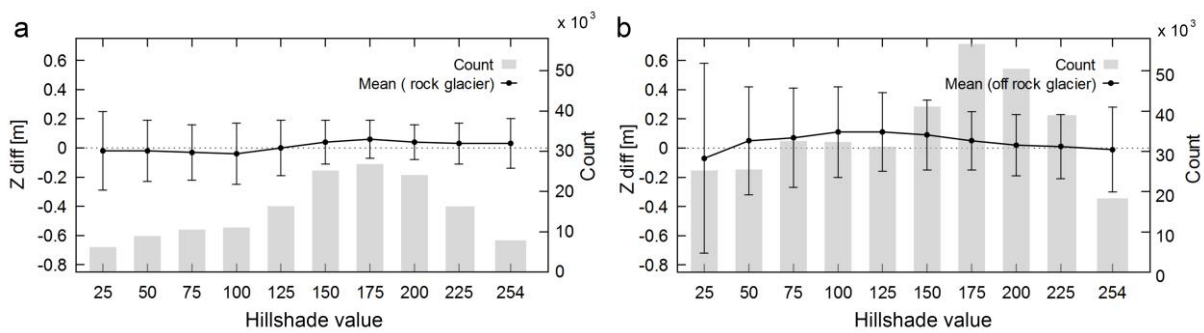
967

968 **Figure 15.** Mean, mean of the absolute values and standard deviation of elevation  
 969 differences between 2014 SfM-MVS and ALS-based DEMs calculated for 10° intervals  
 970 of the slope interval (a) within the reconstructed area of the rock glacier reconstructed  
 971 area and (b) in the bare ground outside the rock glacier.

972

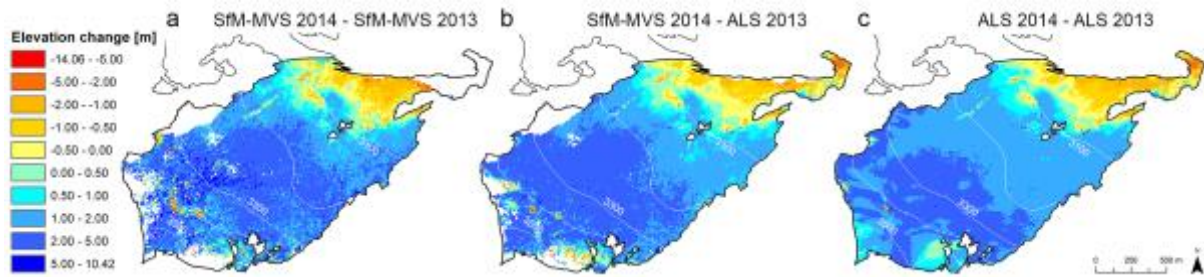


973

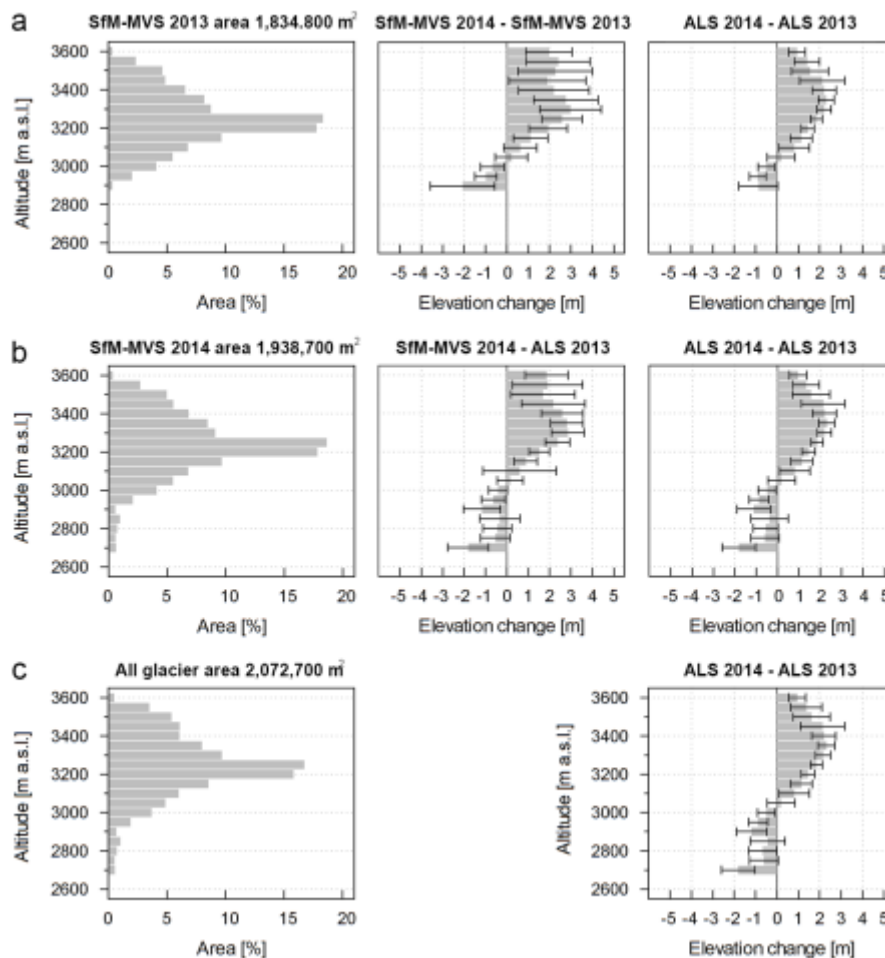


974

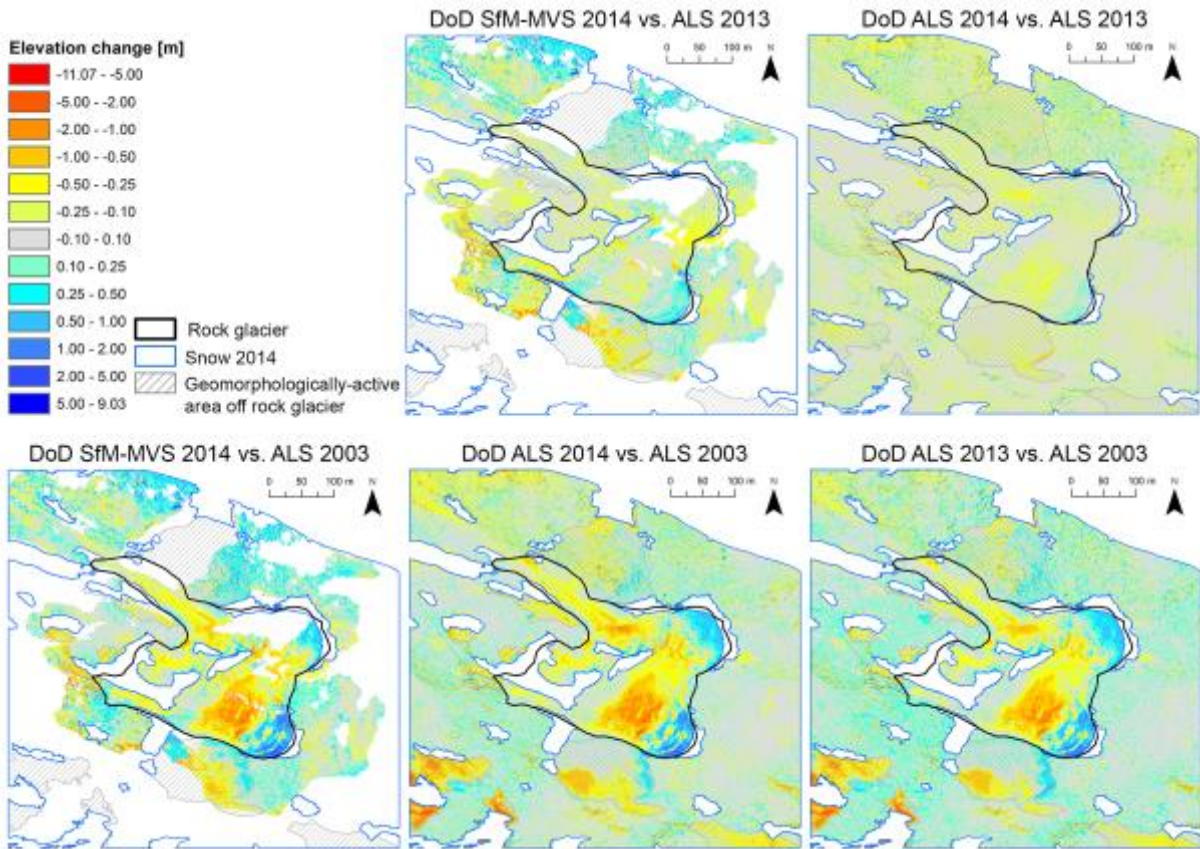
975 **Figure 16.** Elevation differences between 2014 SfM-MVS and ALS-based DEMs  
 976 calculated for ~~the~~ hillshade value intervals of 25 (a) in the rock glacier reconstructed  
 977 area and (b) in the bare ground outside the rock glacier. Lowest values represent  
 978 shadowed area whilst lighted well-lit areas present have the highest values.



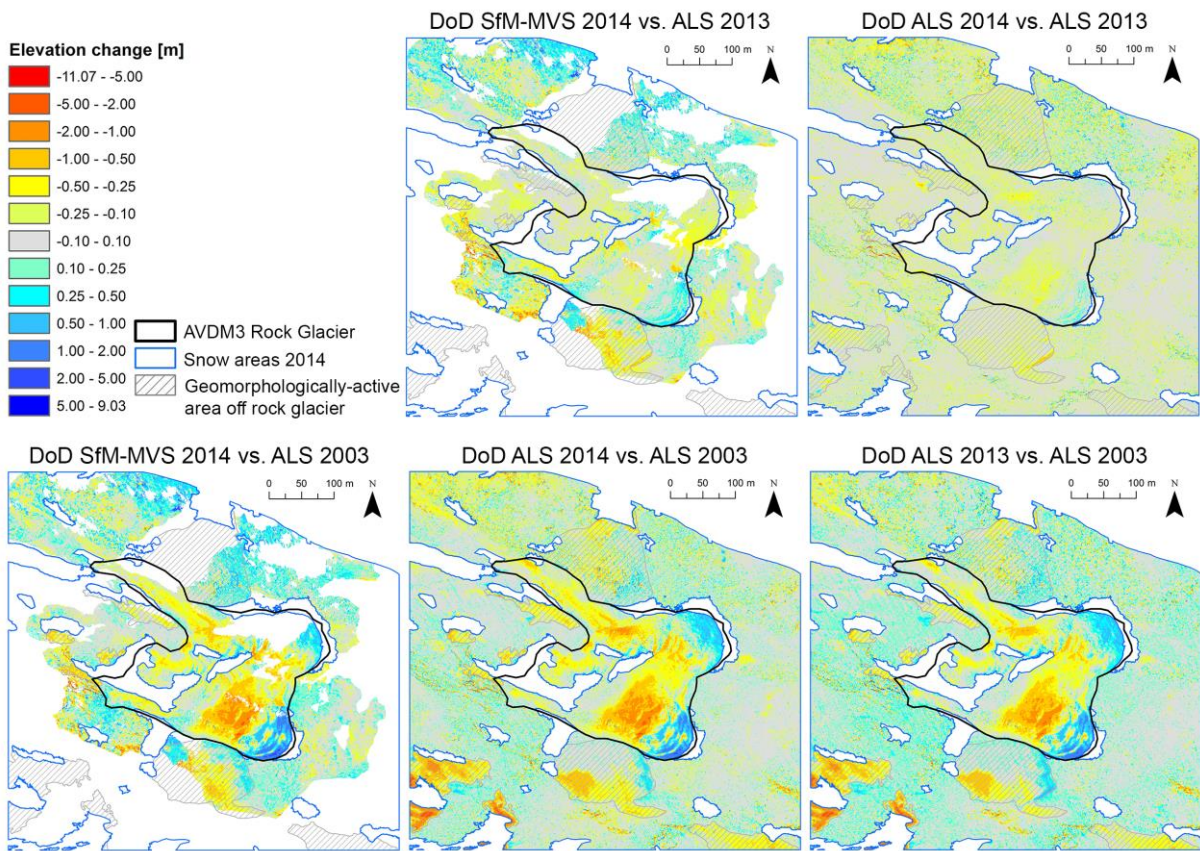
979  
 980 **Figure 17.** Spatial distribution of elevation changes between **(a)** SfM-MVS 2014 and  
 981 SfM-MVS 2013 DEMs **(b)** SfM-MVS 2014 and ALS 2013 over the area of the glacier  
 982 with common coverage and **(c)** ALS 2014 and ALS 2013 over the entire glacier.



983  
 984 **Figure 18.** Area-altitude distribution and surface elevation change with standard  
 985 deviation for the glaciological year 2014/2013 displayed for altitudinal bands with 50 m  
 986 interval. The elevation change were calculated between **(a)** SfM-MVS DEMs of 2013  
 987 and 2014 in the 2013 photogrammetric reconstructed area; **(b)** SfM-MVS DEMs of  
 988 2014 and ALS DEM of 2014 in the 2014 photogrammetric reconstructed area; **(c)** ALS  
 989 DEMs of 2013 and 2014 of the entire glacier. The photogrammetric results were  
 990 compared with the corresponding ALS result calculated in the same area.

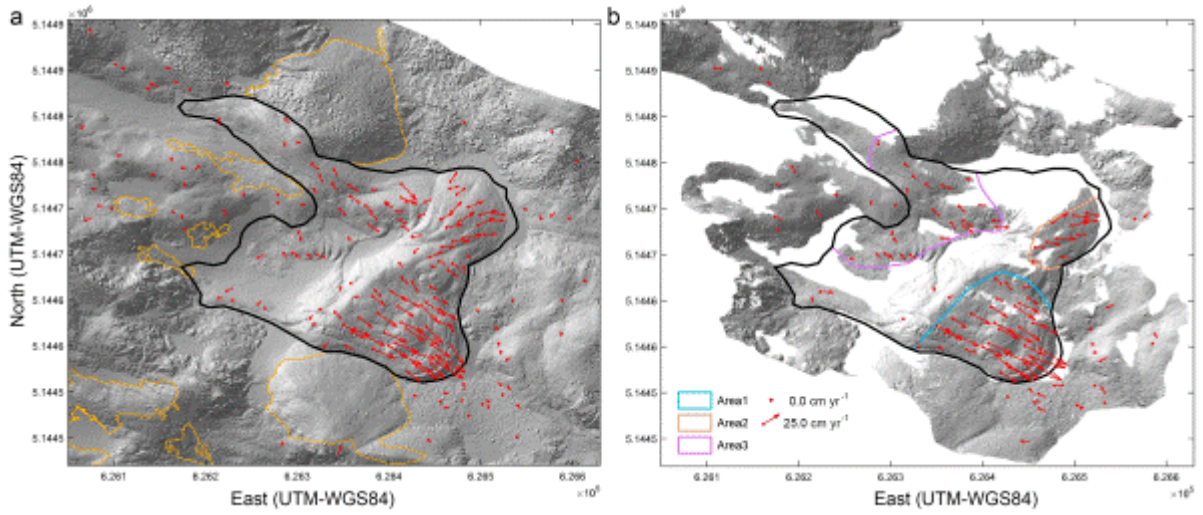


991



992

993 **Figure 19.** Spatial distribution of elevation changes from September 2014 to  
994 September 2013 and September 2003 between the DEMs derived from SfM-MVS and  
995 ALS.



996  
997 **Figure 20.** Displacement vectors of the rock glacier between 2003 and 2014  
998 computed by a manual identification of natural features visible in the hillshaded DEMs  
999 generated by (a) ALS for both survey epochs and by (b) ALS and photogrammetry for  
1000 2003 and 2014 survey, respectively.